FINAL TECHNICAL REPORT

TWO POST-GLACIAL EARTHQUAKES ON THE SADDLE MOUNTAIN WEST FAULT, SOUTHEASTERN OLYMPIC PENINSULA, WASHINGTON

Recipient:
William Lettis & Associates, Inc.
1777 Botelho Drive, Suite 262
Walnut Creek, CA 94596
Phone (925) 256-6070; Fax (925) 256-6076

Principal Investigators:
Robert C. Witter[1], and Robert W. Givler[2]

[1]Oregon Department of Geology and Mineral Industries, Newport Field Office
313 SW 2nd Street, Suite D, Newport, Oregon 97365
Phone: (541) 574-6642; Fax (541) 265-5241
email: rob.witter@dogami.state.or.us

[2]William Lettis & Associates, Inc.,
1777 Botelho Dr., Ste. 262, Walnut Creek, CA 94596
Phone: (925) 256-6070; Fax (925) 256-6076
email: givler@lettis.com

Contributors:
Morgan Zeliff, Christopher Iacoboni, and Robert J. Carson
Geology Department, Whitman College, Walla Walla, WA 99362

Keywords:
Paleoseismology, Surface Deformation, Trench Investigations

Program Elements I

U.S. Geological Survey
National Earthquake Hazards Reduction Program
Award No. 05HQGR0089

2005

Research supported by U.S. Geological Survey (USGS), Department of Interior, under USGS award number 05HQGR0089. The views and conclusions contained in this document are those of the authors and should not be interpreted as necessarily representing the official policies, either expressed or implied, of the U.S. Government.

TABLE OF CONTENTS

ABSTRACT i
1.0 INTRODUCTION 1
2.0 PREVIOUS INVESTIGATIONS 2
3.0 APPROACH 4
4.0 RESULTS 5
4.1 Geomorphic Expression of the Saddle Mountain West Fault 5
4.2 Trench Stratigraphy 5
4.3 Structural Relations 6
4.4 Shallow Cores Near Price Lake 8
4.5 Dating 8
5.0 EARTHQUAKE HISTORY 9
5.1 Earthquake A 9
5.2 Earthquake B 10
5.3 Did an Earthquake Produce the Surface Scarp? 11
6.0 SEISMIC HAZARDS OF THE SADDLE MOUNTAIN FAULT ZONE 13
6.1 Deformation Style 13
6.2 Deformation Rate and Slip Per Event 13
6.3 Rupture Extent and Magnitude 14
7.0 CONCLUSIONS 16
8.0 ACKNOWLEDGEMENTS 17
9.0 REFERENCES 18

LIST OF TABLES

Table 1. Descriptive information for geologic units in Cargill Creek trench

Table 2. Pebble and cobble lithologies from glacial drift exposed in Cargill Creek trench compared to Puget and Alpine drift

Table 3. Field description of soil profile, west wall of Cargill Creek trench

Table 4. Mean pole calculations and 95% confidence intervals for measured clast orientations in glacial till grouped by trench section

Table 5. Radiocarbon isotopic analysis results for detrital charcoal sampled from the Cargill Creek trench, Saddle Mountain West fault

Table 6. Radiocarbon isotopic analysis results for detrital plant macrofossils sampled from sediment cores across Saddle Mountain West fault

Table 7. Fault Displacement, Fold Deformation and Slip Rate Estimates From the Cargill Creek Trench, Saddle Mountain West Fault

LIST OF FIGURES

Figure 1. Tectonic map of western Washington showing crustal faults in the Puget Lowland bound by the Olympic and Cascade Mountain Ranges.

Figure 2. Light detection and ranging (lidar) image of the southeastern Olympic Peninsula near Hoodsport, Mason County, Washington showing northwest-facing scarps of the Saddle Mountain fault zone and recently identified southeast-facing scarps near Frigid Creek.

Figure 3. a) Lidar image of the Price Lake area showing topographic scarps that delineate the Saddle Mountain West, Saddle Mountain East, and Dow Mountain faults previsouly studied by Wilson et al. (1979). b) Topographic map of the Price Lake area showing fault scarps interpreted from lidar image and Quaternary geology modified from Wilson et al. (1979)

Figure 4. Aerial photograph of Saddle Mountain and Price Lake taken in 1939 shortly after extensive timber harvesting.

Figure 5. a) Results of a magnetic survey acquired by canoe on Price Lake (track lines in red) that illuminate a northeast-trending magnetic trough approximately 150m wide that links topographic scarps (white lines) along the Saddle Mountain West fault. b) Two-dimensional model consistent with magnetic data that predicts two east-side-up reverse faults in Crescent Formation at >30 m depth.

Figure 6. a) Simplified Quaternary geologic map (modified from Wilson et al., 1979) of the Saddle Mountain West Fault (SMWF) paleoseismic trench sites and ALSM profile locations. b) Topographic profiles A-E across the SMWF scarps.

Figure 7. Soil profile, west wall of Cargill Creek trench.

Figure 8. Photomosaic (a) and simplified stratigraphy (b) of the northern third of the Cargill Creek trench eastern wall.

Figure 9. Photomosaic (a) and simplified stratigraphy (b) of the central third of the Cargill Creek trench eastern wall.

Figure 10. Photomosaic (a) and simplified stratigraphy (b) of the southern third of the Cargill Creek trench eastern wall.

Figure 11. Lower hemisphere equal area stereonet projections of 89 clast orientation measurements in the Vashon Till.

Figure 12. Photograph showing an offset basalt cobble exposed in the east wall of the Cargill Creek trench with slip indicators consistent with right-lateral oblique reverse displacement on fault F6.1.

Figure 13. Close up photograph of offset cobble showing piercing line used to estimate slip vector.

Figure 14. Stratigraphic profile depicting a 76-m-long sediment core transect across the projected trace of the Saddle Mountain West Fault, located approximately 100-m southwest of Price Lake (see Figure 3).

Figure 15. Schematic reconstruction of earthquake surface ruptures at Cargill Creek inferred from retrodeforming stratigraphic units along faults in the southern part of the trench.

LIST OF PLATES

Plate 1. Trench log of the eastern wall of the Cargill Creek trench.

Plate 2. Photomosaic of the eastern wall of the Cargill Creek trench.

1.0 INTRODUCTION

Too few geological records of Holocene earthquakes exist to reduce large uncertainties in source characterizations for active upper-plate faults in the Puget Sound lowland (Puget Lowland). We investigated the post-glacial earthquake history of the Saddle Mountain West fault, part of a system of northeast-trending, east-side-up reverse faults located on the eastern Olympic Peninsula in Mason County, Washington (Figure 1). These faults, initially identified in the early 1970s, are the first Holocene upper-plate structures recognized in Washington but the details of their seismic potential remain poorly defined. Prominent northwest-facing fault scarps, illuminated by Light Detection and Ranging (LIDAR) vertically offset Vashon till by 1.5 to 4.5 m and suggest that the fault zone is capable of producing large magnitude earthquakes (Figure 2). In addition to the strong motion hazard they pose to the densely populated corridor between Seattle and Olympia, the faults also threaten two Tacoma Power hydroelectric facilities on Lake Cushman and Kokanee Lake.

Prevailing kinematic models suggests that clockwise rotation and northward migration of the Cascadia forearc drives north-south shortening in western Washington as the forearc impinges against the relatively stable Canadian Coast Mountains (Wells et al., 1998). Multiple east-west trending faults (e.g., the Seattle fault), inferred from high-resolution potential field studies, industry borehole data, marine seismic-reflection surveys, and tomographic modeling (Johnson et al., 1994, 1999; Pratt et al., 1997; Brocher et al., 2001; Blakely et al., 2002), accommodate north-south contraction within the Puget Lowland. Although geodetic data confirm northward propagation of the Cascadia forearc (Kazaradze et al., 1999; Miller et al., 2001), complexities in the pattern of seismogenic strain show evidence for localized northwest-southeast crustal shortening and thickening near Hood Canal in the eastern Olympic Peninsula (Lewis et al., 2003). The Seattle and Tacoma faults, east-west structures that cross the Puget Lowland, appear to terminate against the eastern Olympic Peninsula along northeast-trending structures that include the Saddle Mountain fault zone and the inferred Hood Canal fault. Johnson et al. (1994), for example, noted that the Seattle fault zone appears to be truncated by the Hood Canal fault—a fault previously identified by Gower et al. (1985) as the eastern margin of a northeast-trending gravity high that probably reflects steeply-east dipping Crescent Formation basalt of middle and lower Eocene age. The Saddle Mountain fault zone appears to be the surficial expression of the southern part of this gravity anomaly and evidence for east-side-up deformation reveals more complex patterns of deformation not explained by simple models of north-south shortening, highlighting the importance of comparisons between the geologic record and contemporary strain patterns.

This report presents the results of paleoseismic trenching across the Saddle Mountain West fault near Cargill Creek on the northern flank of Dow Mountain (Figure 3). Surface rupture during two post-glacial earthquakes is deduced from trench exposures showing faults that offset glacial till and outwash of the Vashon stade (18 to 13 ka) of the Fraser glaciation as well as overlying Holocene slope colluvium. In addition, we report the first evidence for a right-lateral slip component on a shallow reverse fault in the Puget Lowland, estimate a post-glacial vertical deformation rate, and present empirical data that suggest the Saddle Mountain fault zone is capable of producing M_w 6.5 to 7 earthquakes.

2.0 PREVIOUS INVESTIGATIONS

Carson (1973) first reported the presence of earthquake-related fault scarps on Saddle Mountain, in Mason County, Washington, although the linear surface expression of the faults in a landscape denuded by timber harvesting before 1939 (Figure 4) was probably recognized by earlier workers (Wilson, 1975). Wilson (1975) developed a detailed geologic map and documented Pleistocene or younger movement on three reverse faults in the area, including the Saddle Mountain West fault, the Saddle Mountain East fault, and the Dow Mountain fault (Figure 3). Carson and Wilson (1974) proposed that the linear, northeast-trending Cushman Valley, northwest of Dow Mountain, reflects a fourth potential late Quaternary fault in the area. LIDAR data show that the Cushman Valley lineament is aligned with prominent scarps directly to the northeast suggesting that the linear valley is the southwestern expression of the Saddle Mountain East fault. Trenches excavated across the scarps in the early 1970s exposed faults that offset Vashon glacial deposits, scarp colluvium interlayered with pre-Fraser age till (>30 ka), and Crescent Formation bedrock (Wilson et al., 1979).

Wilson (1975) excavated a trench across the West fault on the southern side of Saddle Mountain where it forms a 3.9-m high scarp (Figure 3b). Wilson et al. (1979) report that trench exposed a 1.8-m high, east-side-up, buried scarp in Crescent volcanics. To the west, scarp colluvium interlayered with pre-Fraser till abuts the basalt. Vashon till mantles the entire section and appears to be warped above the buried scarp. Although the trench was not deep enough to expose the fault in bedrock, Wilson et al. (1979) assumed that the height of the buried basalt scarp (1.8 m) represented the vertical component of fault slip along a fault plane striking N19°E, and dipping 67°SE. Wilson et al. (1979) inferred at least two episodes of movement on the West fault. An earthquake probably occurred during a pre-Fraser glaciation evident by scarp colluvium interlayered with pre-Fraser age till. Topographic expression of the scarp in Vashon age till suggests that the most recent earthquake occurred after retreat of the Puget lobe of the Cordilleran ice sheet about 14 ka (Porter and Swanson, 1998). Wilson et al. (1979) imply that surface rupture produced by the most recent event may have impounded Lilliwaup Swamp about 8,715 ± 185 ^{14}C yr BP based on radiocarbon analysis of wood from an organic layer buried below the wetland. They estimate a minimum fault length of 3.2 km from scarp expression on Saddle Mountain and its northward projection along the eastern margin of Lilliwaup Swamp.

Wilson (1975) excavated two trenches across the Saddle Mountain East fault. The northern trench is located on the south side of Saddle Mountain across a 3-m high scarp. The southern trench crosses a 4.5-m high scarp on the south side of Price Lake and now serves as a fishing access trail. In the report by Wilson et al. (1979), the fault exposed in the northern trench strikes N22°E and dips 75°SE and vertically offsets the contact between Crescent Formation basalt and overlying Vashon till by 3.5 m. Striations on the fault surface show a rake of 66° to the southeast indicating a component of left-lateral motion. Evidence of fault-related deformation in the southern trench includes complexly folded and faulted Vashon drift (Wilson, 1975). Carson (1973) proposed that east-side-up surface displacement produced by the most recent earthquake impounded water west of the scarp, forming Price Lake and drowning a forest. Radiocarbon dates on material from stumps in Price Lake and a pond on the northeast side of Saddle Mountain suggest that the trees were submerged about 5,100 ± 500, 1,315 ± 80, and 1,155 ± 85 ^{14}C yr BP (Wilson et al., 1979). An additional radiocarbon date of 1,600 ± 200 ^{14}C yr BP on charcoal from colluvium in the footwall of the fault exposed in the northern trench provides further evidence for late Holocene faulting. However, Wilson et al. (1979) could not conclusively demonstrate whether the ages represented one or more earthquakes.

Fault gouge, fractured basalt and offset pre-Fraser drift were observed in a trench across a 7.6-m high scarp on Dow Mountain (Carson and Wilson, 1974; Wilson, 1975). The Dow Mountain fault strikes N58°W, dips 59°NE and is nearly perpendicular to the Saddle Mountain fault zone (Figure 3b). The fault

vertically offsets a layer of sandy gravel separating deposits of pre-Fraser till by 1.7 m providing evidence for at least one earthquake after the pre-Fraser glaciation.

Drowned tree stumps rooted in a forest soil submerged below Price Lake and buried beneath surrounding wetlands investigated by Hughes (2005) suggest surface rupture of both the West and East faults between 1,000 and 1,300 cal yr BP. Radiocarbon analyses of cones and needles from the ancient soil in the footwall of both faults provide statistically similar ages that closely limit the time of faulting. Further evidence that both faults ruptured within the span of two centuries comes from cross-dating of the annual rings of drowned, growth-position Douglas Fir stumps, the relative degree of weathering of stump tops, and their consistent elevations with respect to the current lake-surface level. Hughes (2005) used the heights of growth-position stumps in the lake and the highest elevation of the soil in which they were rooted to estimate the vertical component of displacement produced by the most recent surface ruptures. Vertical offset probably exceeded 4 m on the East fault and 2 m on the West fault.

Aeromagnetic data, processed to highlight the shallow crustal structure of Crescent Formation basalt in the Saddle Mountain fault zone, reveal anomalies that reflect north-northeast-trending, east-side-up faults that extend from Lake Cushman at least 18 km north to the Hamma Hamma River (Blakely et al., 2005). In the same study, detailed magnetic surveys of the West fault beneath Price Lake image a northeast-trending, 150-m wide, linear magnetic trough aligned with LIDAR scarps on the northern and southern lake shores (Figure 5a). Simple, two-dimensional models of the anomaly suggest that two southeast-dipping reverse faults with >20 m of displacement offset the Crescent Formation at >30 m depth (Figure 5b). The inferred displacements at depth are significantly larger than vertical slip estimates from scarp heights (1 to 10 m) and trench investigations (1.8 to 3.5 m) (Wilson et al., 1979). Additional prominent anomalies evident in ground-magnetic data studied by Blakely et al. (2005) are not coincident with topographic scarps and may reflect concealed structures within a complex zone of faulting.

3.0 APPROACH

A 17-m long trench, named the Cargill Creek trench, excavated across the Saddle Mountain West fault scarp south of Price Lake exposed faulted Vashon glacial till, stratified ice-contact drift and overlying post-glacial colluvial deposits (Trench 1, Figure 6). Trench exposures were cleaned, strung with a 1x1 m grid, digitally photographed, and logged at approximately 1:20 scale (Plate 1). A digitally-rendered photo-mosaic (Plate 2) registered to the metric grid provides an objective, uninterpreted view of the eastern trench wall as a basis for stratigraphic and structural interpretations shown on the trench log.

A second 13-m long trench, located approximately 50-m northeast of the first trench, exposed probable Holocene alluvial gravel and sand deposits but was immediately backfilled because of unstable excavation conditions (Trench 2, Figure 6).

Detailed lithologic descriptions of trench strata are shown in Table 1; abridged descriptions of lithologic units are shown on the trench log (Plate 1). The origin of glacial till was inferred from cobble lithologies from the trench shown in Table 2. Soil descriptions (Figure 7) followed the methodology of the USDA Soil Survey (Schoeneberger et al., 2002).

Cobbles and pebbles cemented in glacial till (unit 1) were measured to evaluate possible earthquake-related folding of an apparent cobble fabric. We measured the strike and dip of the exposed long-axis of all large cobbles and pebbles ($n = 89$, ≥ 4 cm) in the east and west trench exposures. A discussion of cobble orientation results is given below.

A stratigraphic profile across the West fault, obtained using a 2-cm diameter, hand-driven gouge corer, provides preliminary constraints on vertical separation of the contact between probable post-glacial outwash deposits and overlying late Holocene wetland and lacustrine deposits. The 80-m long core transect was positioned perpendicular to a subdued east-side-up step in topography aligned with the projected trace of the Saddle Mountain West fault scarp southwest of Price Lake. Ten sediment cores revealed interbedded forest soils, wetland peat and soft silt to sandy silt overlying impenetrable gravel deformed within the scarp.

Isotopic analyses of radiocarbon (^{14}C) using accelerator mass spectrometer methods dated organic material from the trench and cores. Calibrated ^{14}C dates were used to estimate deposit ages and, where deformed in the scarp, the time of faulting. Samples analyzed included detrital charcoal sampled from colluvial deposits in the trench and fossil plant remains from buried peat observed in shallow cores near Price Lake. Lab reported ages were calibrated with CALIB v. 5.0.2html software (Stuiver and Reimer, 1993) using the calibration dataset of Reimer et al. (2004), an error multiplier of 1, and reported to two standard deviations of the mean.

4.0 RESULTS

4.1 Geomorphic Expression of the Saddle Mountain West Fault

Prominent geomorphic lineaments resolved by LIDAR-generated shaded-relief maps and historical aerial photography from 1939 define the 4- to 5-km-long surficial expression of the Saddle Mountain West fault (Figures 3 and 4). The lineaments include a northeast-trending series of scarps that extends from the northwestern flank of Dow Mountain on the south, across the Price Lake basin and over Saddle Mountain, to Lilliwaup Swamp on the north (Figure 2). Near Cargill Creek north of Dow Mountain (Figure 6), a single, 1- to 2-m-high, east-side-up scarp deforms Vashon glacial till and outwash deposits and post-glacial alluvial deposits. The scarp trends N50°E and is concealed beneath Price Lake and surrounding latest Holocene alluvial, wetland and lacustrine deposits (Figure 3). However, tonal contrasts evident in 1997 aerial photography and field inspection of drowned stumps reveal an increase in lake depth to the west of where the scarp projects beneath the water, indicating deformation of the lake floor. Northeast of Price Lake multiple topographic lineaments, including both east- and west-facing scarps, trend N20°-25°E and climb the southern flank of Saddle Mountain toward the graben-like cleft in the ridge that defines its name (Figure 3). A 3.9-m-high west-facing scarp coincides with the eastern edge of the topographic saddle and an east-facing scarp coincides with the western edge of the saddle. North of Saddle Mountain, the scarps project toward the eastern linear termination of Lilliwaup Swamp that is impounded by topographically higher Vashon glacial till to the east (Figure 3).

4.2 Trench Stratigraphy

Stratigraphic units encountered in the Cargill Creek trench include both glacial (latest Pleistocene) and post-glacial (Holocene) deposits that underlie a gentle, northward-sloping geomorphic fan previously mapped by Wilson (1975) as Vashon recessional outwash (Figure 3 and 5). The detailed log of the eastern trench wall shown in Plate 1 represents our stratigraphic interpretation of the trench exposure. Plate 2 shows an uninterpreted photomosaic of the eastern trench wall. Detailed lithologic descriptions of each stratigraphic unit are included in Table 1 and summary unit descriptions are shown on Plate 1. The following section briefly describes the nature of the deposits observed in the Cargill Creek trench and the basis for our stratigraphic interpretation.

The oldest deposit is a densely-cemented diamicton composed of sandy, silty gravel (unit 1a) that includes irregularly-shaped, discontinuous lenses of weakly stratified sand and gravel (unit 1b) and rare cobbles of granite, diorite and quartzite lithologies (Plate 1, Table 2). We interpret the diamicton to be latest Pleistocene glacial till of the Vashon stade of the Fraser glaciation. Descriptions of similar deposits mapped in the southern Olympic Peninsula distinguish Vashon till produced by the continental ice sheet from Olympic till produced by alpine glaciers by the presence of granite, diorite and quartzite clasts that are exotic to the Olympic peninsula (Carson, 1970 and 1976; Wilson, 1975).

Locally (between horizontal stations 13 m and 15 m, Plate 1), discontinuous relict deposits of stratified sand, silt and gravel (unit 2) overlie the till (unit 1). These layered deposits have been preserved along a fault-bound block that dropped below the maximum depth (~0.75 m) of mixing caused by slope processes that have destroyed original stratification elsewhere. We interpret deposits of unit 2 to be latest Pleistocene ice-contact stratified drift or glacial outwash. Stratified glacio-fluvial outwash agrees with previous mapping by Wilson (1975) and Carson (1976) that identifies Vashon recessional outwash beneath a broad alluvial fan incised by Cargill Creek (Figure 3).

Several stratigraphic packages of mixed gravel, sand and silt (units 3 to 9) overlie the glacial deposits (Plate 1). These deposits reflect post-glacial colluvial and soil processes on a forested slope, scarp

collapse and erosion, and 20th century logging activities. Colluvial deposits of units 3 and 4 consist of yellowish-brown gravel, sand and silt principally derived from glacial deposits. Buried, north-dipping colluvial packages of unit 5 are derived from glacial till and unit 3 and produced by collapse and erosion of a fault scarp possibly modified by a large tree-throw crater located at the base. Units 6, 7 and 8 include colluvial deposits filling tree-throw craters, mixed by root stirring, and disturbed by logging activities. Unit 9 represents modern A and O soil horizons that consist of very dark brown to black gravelly, sandy silt and forest litter. We infer a younger relative age for unit 7 deposits formed by tree-throw because the feature has not been obliterated by recent slope processes that mix and homogenize other shallow colluvial deposits.

A soil profile exposed in the western wall of the Cargill Creek trench (Figure 7), and described in Table 3, shares many characteristics of the Alderwood and Hoodsport soil series in Mason County mapped by Ness et al. (1960). Soil development for the Alderwood and Hoodsport series is influenced by high annual rainfall (1,500 to 2,500 mm) and glacial parent material that includes strongly cemented Vashon till with abundant, locally-derived basalt clasts. From the ground surface, the upper 5 to 10 cm of the profile consists of an O horizon composed chiefly of forest litter with abundant roots. A very dark brown, silt-rich A horizon, about 15 cm thick, underlies the O horizon. A strong brown Bw horizon in sandy loam and gravel grades downward to a gravelly BC horizon with finer matrix material that, together, extend from about 22 to 73 cm depth. The A and B soil horizons are characterized by weak, fine to medium, blocky peds and common roots that generally decrease in abundance with depth. Very dark grayish brown, single-grained sand and gravel, interpreted as oxidized colluvium directly overlying glacial till, comprises the 1Cox horizon. Deeper soil horizons developed in the till include the 2Cox1 and 2Cox2 horizons that consist of dark yellowish brown and very dark grayish brown, well-cemented sandy gravel, respectively. The most notable characteristic of the 2Cox1 horizon is a coarse, well-developed, platy structure within the upper 10 cm of the till. Similar soil structure has been described in C horizons developed in till of the Alderwood series (Ness et al., 1960). The platy structure developed within the till in the Cargill Creek trench provided a useful strain gauge that we used to estimate the vertical component of deformation.

4.3 Structural Relations

The Cargill Creek trench exposed a 10-m wide deformation zone characterized by steeply-dipping, northeast-striking faults and fractures that offset glacial and overlying colluvial deposits (Plate 1). The total vertical separation of the contact between glacial till and overlying colluvium across the entire deformation zone is about 1 m. Total vertical relief of the land surface is approximately 1.7 m, measured by the vertical separation of the hillslope across the scarp, suggesting that folding accommodated some of the deformation. Structural relations observed in the trench are summarized below. Each fault or fracture is identified by a number (Plate 1) and grouped into zones of concentrated deformation where faults and fractures are closely-spaced and, in some cases, interconnected (Figures 8, 9 and 10). In addition, this section describes the preferential alignment of cobbles in till that reflect fold deformation (Figure 11) and presents possible evidence for a lateral slip component based on measurements of an offset basalt cobble in the western trench wall (Figures 12 and 13).

In the northern third of the trench two faults and associated fractures disrupt unit 1 and fault F2 offsets the contact between glacial till and overlying colluvium (Figure 8). Fault F1 is an inferred discontinuity coincident with an apparent 10-cm, south-side-up vertical separation of the lower boundary of the 1dCox soil horizon. However, an opposite sense of vertical separation across the base of unit 1b and equivocal evidence for vertical separation across the contact between till and overlying colluvium suggest that if F1 is a fault then it has accommodated primarily lateral slip (see note n8, Plate 1). Fault F2 offsets both Vashon glacial till (unit 1) and the overlying colluvium (unit 4a), but is not coincident with a surface scarp. Fault F2 vertically separates the contact between till and colluvium by about 0.3 m (north side

down) along a plane that strikes N 54° to 64° E and dips 61° SE. Possible secondary faults and fractures splay upward from fault F2, including F2.3 that terminates at a downward-tapering fissure filled with colluvium of unit 4 (see note n9, Plate 1).

Two zones of deformation in the central part of the trench, F3 fractures and fault zone F4, bound the northern and southern margins of a prominent bowl-shaped depression filled with scarp colluvium that directly underlies the surface fault scarp resolved on LIDAR (Figure 9). The F3 fractures consist of a series of discontinuous, aligned voids within the till (unit 1) that are coincident with the apparent vertical separation of unit 1b below the base of the surface scarp. Fault zone F4 is located directly below the top of the surface scarp and includes both northwest and southeast dipping faults and fractures, many aligned with voids in the till and extensional cracks (unit 1). Measured strikes and dips on F4 fractures range from N 70° E, 80° SE to N 80° E, 54° NW. The northern-most fault in fault zone F4 is a planar zone of friable, disintegrated silty sand within otherwise dense, compact till below the base of the surface scarp. All faults and fractures within the zone appear to terminate within the till or at the contact between till and overlying colluvium. However, stacked, scarp-derived colluvial wedges (units 5a and 5b) that overlie fault zone F4 and lap onto colluvium of unit 3 suggest that fault F4 have accommodated primary fault rupture that offset unit 3 and produced a scarp that has since degraded through collapse and erosion. Secondary faults F4.1 to F4.4 may have accommodated hanging-wall deformation and/or abetted post-earthquake gravitational collapse of the scarp. An alternative hypothesis for the origin of the scarp colluvium involves tree throw. As we discuss later, regardless of its genesis, the timing of the event that formed the bowl-shaped excavation in till remains elusive because of the scarcity of detrital charcoal in unit 5a.

The southern third of the trench exposed two zones of faulting (F5 and F6) that bracket a down-dropped block of till and overlying stratified glacial drift of unit 2 (Figure 10). Faults within both zones strike east-northeast with dips ranging from 50° to 80° SE; fractures in fault zone F6 have similar strikes and dip to the northwest. Faults F5.1, F5.2 and F6.1 offset glacial till (unit 1), stratified drift (unit 2) and the basal contact of colluvium in unit 3aCox. Vertical separation of the top of glacial till along fault F5.2 and fault F6.1 is about 0.2 m and 0.5 m, respectively. Cobbles in unit 3 colluvium near the upward termination of these faults are rotated about axes parallel to fault strike and indicate displacement of unit 3aCox and unit 3bBC (see note n24, Plate 1). Shearing along these faults may have accommodated slight clockwise rotation of individual blocks causing back-tilting along the upper till contact. Subtle warping along the basal contact of unit 3bBC may reflect slumping into the graben or root-stirring.

Measured axial planes of oblate cobbles in glacial till exposed in the eastern and western trench walls were examined to evaluate evidence of possible warping or folding of an apparent cobble fabric in the till (Table 4). Calculations of the mean poles of cobble axial planes show a consistent fabric in the till expressed by cobbles oriented with a preferential dip of 50° ± 20° in a northward direction. Stereonet projections were plotted for mean poles of 89 cobbles and grouped by horizontal distance along six sections of the trench. The 95% confidence intervals for each group show substantial overlap and suggest that cobble orientations are statistically similar across the entire trench (Figure 11a). A Kamb plot of all calculated poles shows a consistent pole concentration in the southern quadrant that reflects a general east-west striking, northward-dipping cobble fabric in the till (Figure 11b). Considering the uncertainty in cobble orientations, if earthquake-related warping or folding has deformed the till, then any possible change in the cobble fabric was probably less than 20°.

Possible evidence for a right-lateral component of slip comes from an offset basalt cobble observed in the west wall of the trench (Figures 12 and 13). The fault that offsets the cobble is aligned with fault F6.1 in the east wall (Plate 1). Both fragments of the offset cobble were firmly cemented in glacial till and showed no evidence of rotation. The intersection of a linear groove on the cobble surface with the fault plane striking N 47° E and dipping 58 S provided a piercing point to estimate a slip vector (Figure 13).

Direct measurement of the piercing point yields a displacement estimate of 7.5 cm along a slip line with a rake of 51° to 56° NE. These data indicate right-lateral oblique reverse displacement of the cobble with a 1.5:1 horizontal to vertical slip ratio. The small magnitude of displacement suggests the cobble was split by secondary deformation and its slip vector may not reflect movement on the main fault.

4.4 Shallow Cores Near Price Lake

A 76-m-long stratigraphic profile (Figure 14) of wetland and lacustrine sediments was constructed from a field transect of 10 sediment cores located approximately 100 m south of Price Lake (Figure 3) and oriented perpendicular to the Saddle Mountain West scarp. Stratigraphic sequences observed in the cores reflect a general thickening of sediments toward the northwest consistent with south-side-up deformation across the scarp. This section describes the stratigraphic and structural relations interpreted from the profile and used to infer possible fault-related deformation beneath the scarp.

Five lithostratigraphic units were identified in the cores (Figure 14). Six cores met refusal on dense, cemented and oxidized gravel inferred to be glacial outwash deposits. Younger deposits include discontinuous beds and lenses of sandy to gravelly mud intercalated with silty mud, peat and muck. Other discontinuous layers consist of organic mud similar to lake sediment. These post-glacial deposits that overlie possible glacial outwash reflect sedimentation in a wetland or lake similar to the present low-lying forest and marsh environments that surround Price Lake.

Northwestward-thickening sediments overlying dense gravel may reflect post-glacial fault-related deformation or fluvial scouring that formed the buried scarp shown in the stratigraphic profile (Figure 14). If formed by faulting, two earthquakes are evident from the increasing vertical separation of strata with depth. Separation of the top of glacial outwash deposits is about 1.8 m; whereas, vertical relief across the scarp at the surface is about 0.5 m. The equivocal evidence for fault-related deformation in the stratigraphic profile is consistent with evidence for two earthquakes in trench exposures and suggests that significant aggradation of wetland and lacustrine sediment took place after each event. Alternatively, aggradation of the sediment may have filled an abandoned fluvial channel that modified the fault scarp or formed a different scarp in the landscape unrelated to faulting.

4.5 Dating

^{14}C analyses of six charcoal fragments sampled from trench strata provide stratigraphically consistent age estimates to constrain the timing of fault-related deformation (Table 5). Charcoal, probably produced by forest fires, may have long residence times and likely represent maximum ages of the hosting colluvial deposits. An early Holocene age (8,380 to 8,540 cal yr BP) came from charcoal located near the base of the colluvial soil (unit 3aCox) that overlies till on the uphill side of the scarp. Other ages derived from charcoal in stratigraphically higher units were much younger. Two statistically indistinguishable age estimates ranging from 1,560 to 1,810 and 1,630 to 1,860 cal yr BP suggest that unit 3cBw above the scarp and unit 4a below the scarp were deposited contemporaneously. Alternatively, charcoal in unit 4a could be significantly older than the time of deposition if it was recycled from older sources. Charcoal in scarp colluvium of unit 5b ranged from 1,360 to 1,530 cal yr BP. The two youngest ages come from unit 4bBw and ranged from 800 to 1,050 and 1,180 to 1,390 cal yr BP.

Dates of plant remains estimate the ^{14}C age of peaty wetland sediments that spans the fault scarp where it projects toward the southwestern shore of Price Lake (Table 6). Peat from a core on the northwest (down-thrown) side of the scarp dated to 8,420 to 8,590 cal year BP. Detrital seeds carefully picked from peat on the southeast (up-thrown) side of the scarp provided a slightly younger age of 8,040 to 8,330 cal yr BP (Figure 14).

5.0 EARTHQUAKE HISTORY

Our interpretation based on retrodeformation of stratigraphic and structural relations in the Cargill Creek trench supports a history of two Holocene earthquakes on the Saddle Mountain West fault (Figure 15). Both earthquakes vertically displaced the basal contact of post-glacial colluvium and underlying Vashon glacial deposits. From this, we infer that both episodes of faulting ruptured the ground surface above multiple offsets of the base of colluvium of 0.3 to 0.5 m. However, if the surface ruptures formed wedges of scarp colluvium, surface fissures or other fault-related features, the evidence largely has been erased because slope processes have mobilized and mixed deposits within 0.5 to 0.75 m of the surface. Exceptions are two wedge-like packages of colluvium (units 5a and 5b), derived from a buried scarp formed in glacial till, that fills a bowl-shaped depression located directly below the surface scarp. We consider both surface fault rupture and root throw as possible explanations for the origin of the buried scarp and its subsequent degradation that formed the colluvial wedge and the surface scarp. Constraints on the timing of earthquakes come from maximum-limiting ^{14}C ages on detrital charcoal in deposits that bracket event horizons and the initiation of ice retreat in the Puget Lowland. The ages provide only broad constraints on the time of the oldest earthquake, placing it before ~8.5 ka but after ~17 ka. Younger ages distinguish the most recent event from its predecessor and constrain the time of faulting to after ~1.7 ka, but ages on detrital charcoal cannot provide a more precise estimate of the time of rupture. Although imprecise, maximum age constraints on the most-recent event are consistent with rupture of the West fault about 1,000 to 1,300 cal yr BP inferred from drowned trees in Price Lake and submergence of a forest soil (Hughes, 2005).

5.1 Earthquake A

Evidence for the earlier of the two events, earthquake A, comes from a down-dropped, fault-bound block that preserves relict layers of stratified gravel and sand interpreted as Vashon recessional outwash or ice-contact stratified drift (unit 2) (Figure 15). As the only remains of stratified deposits from what was probably an extensive outwash fan (Qvr, Figure 3), the unique isolation of unit 2 between faults F5.2 and F6.1 and its consequent protection from the mixing effects of slope processes, distinguishes earthquake A from the most recent event. Because unit 2 is solely preserved in the fault block and conspicuously absent elsewhere in the trench, we infer that earthquake A occurred some time after ice retreated from the area but before mixing by slope and soil processes could destroy the layered features of stratified drift. Colluvial mixing probably erased evidence of scarp-derived colluvial packages and surface expression of fault rupture.

Inexact constraints on the timing of earthquake A come from estimates of the onset of recession of the Puget lobe of the Cordilleran ice sheet and a ^{14}C age on detrital charcoal from the base of the colluvial deposit (unit 3) overlying unit 2. We place the maximum time of faulting to sometime after 16.7 to 17 ka during the initial period of rapid ice retreat in the southern Puget Lowland (Porter and Swanson, 1998). The minimum age constraint on surface rupture comes from colluvium (unit 3aCox) overlying unit 2 that hosts detrital charcoal with an age of 8,380 to 8,540 cal yr BP. The faults truncating unit 2 also offset the base of the colluvium, which we infer records a second, younger event because (1) the base of unit 3 is displaced less than half the offset of the top of the till, and (2) soil processes on a forested slope destroyed stratification in unit 2 adjacent to the fault block after earthquake A. Although they only broadly estimate the time of faulting, the stratigraphy and ages suggest earthquake A occurred between ~17 ka and ~8.5 ka.

Slip estimates on faults triggered by earthquake A are deduced from the apparent vertical offset of the top of unit 1. Apparent north-side-down displacement across fault F6.1 amounts to dip-slip of about 0.4 m. About 0.15 m of slip in the opposite direction occurred on fault F5.2 that borders the north side of the graben. Differential slip along the two faults may have been accommodated by back-tilting of the graben

(Figure 15). The sum of displacements related to dip-slip and tilting across the graben results in negligible overall offset of the top of till between 0 and 0.1 m. The amount of lateral slip that may have accompanied earthquake A, if any occurred, could not be determined from the outcrop.

Additional slip during earthquake A may have contributed to the formation of the LIDAR scarp, but we found no way to estimate this deformation. Clearly, the 0 to 0.1 m net offset across the top of till did not produce the pronounced 1.7-m high scarp revealed by LIDAR (Figure 3a). Such a minor feature in the topography was likely short-lived and quickly overwhelmed by the churning forces active on a forested slope. Later in this section, we speculate on the origin of the enigmatic LIDAR scarp.

5.2 Earthquake B

Interpretations of offset strata document a younger event, earthquake B, that triggered fault slip in both the northern and southern parts of the Cargill Creek trench (Figures 8 and 15; Plate 1). The most prominent expression of this event was observed in the northern part of the trench where fault F2 vertically displaces the base of colluvium over till and marks a north-side-down vertical step that juxtaposes unit 1 against unit 4a (Plate 1; Figure 8). Secondary faults and fractures that splay off of fault F2, also probably formed during earthquake B. One of these fractures (F2.3) coincides with a downward-tapering fissure filled with colluvium that penetrates the till. Fault F1, also possibly activated during earthquake B, appears to vertically offset the base of an oxidized C-soil horizon (1dCox) developed in the upper part of the till. However, an opposite sense of displacement of the lower boundary of unit 1b presents uncertainty regarding the direction of vertical displacement. If fault F1 expresses north-side-down displacement like fault F2, then the apparent vertical offset of unit 1b may instead reflect a component of lateral displacement that placed a thicker part on the south against a thinner part of the same unit on the north. Because unit 1b is discontinuous and was not observed in the west trench wall, we cannot speculate on the direction of possible lateral motion.

Detrital charcoal fragments from units in both the northern and southern parts of the trench give consistent maximum-limiting ^{14}C age estimates for the time of earthquake B. Therefore, we prefer the simplest explanation that only one earthquake followed event A, rather than two separate events that triggered slip on faults in the northern and southern parts of the trench independently. In the south, an age from the BC-soil horizon (unit 3bBC) places deformation after 1,630 to 1,860 cal yr BP. In the north, dates from units 4a and 4bBw that most closely bracket the event horizon can only yield maximum-limiting age constraints. The maximum age spans 1,560 to 1,810 cal yr BP for unit 4a cut by fault F2. Younger ages from unfaulted unit 4bBw, although consistent with their stratigraphic position, may not provide a minimum age constraint because the charcoal may have been reworked from older deposits exposed in the primary scarp upslope. Nevertheless, the two ages, ranging from 1,180 to 1,390 and 800 to 1,050 cal yr BP, overlap a narrower age estimate reported by Hughes (2005) for the most recent earthquake that may have simultaneously ruptured both the East and West strands of the Saddle Mountain fault zone. From this supporting data, and lacking any evidence to the contrary, we infer that the most recent event recorded in the Cargill Creek trench represents the same earthquake that dammed Price Lake and drowned a forest 1,000 to 1,300 cal yr BP.

Measured displacements on faults triggered by earthquake B give slip estimates from apparent vertical offsets of the top of unit 1 and an obliquely-offset cobble that requires a component of right-lateral displacement. In the northern part of the trench, less than 0.1 m of north-side-down dip-slip displacement is evident on fault F1. Lateral motion on this fault could explain the lack of conclusive evidence of vertical offset. Fault F2 contributes an additional 0.3 m of dip-slip. A north-side-down vertical component of slip on fault F2.4 could be as much as 0.2 m, although we found no obvious stratigraphic offset. Alternatively, deformation not accommodated by faulting could be accounted for by warping or tilting

otherwise not evident in the massive till. Total offset across all three faults in the zone sums to 0.5 to 0.6 m of dip slip along a fault with attitude similar to fault F2.

At the south end of the trench, faults F5.2 and F6.1 accommodate 0.1 and 0.2 m of antithetic dip-slip, respectively, not including the prior displacement produced by earthquake A. Back-tilting of the till sliver between faults F5.1 and F5.2 accounts for about 0.1 m of south-side down deformation. Total dip-slip displacement across all three faults amounts to less than 0.1 m to zero. The oblique offset of a cobble firmly cemented in glacial till indicates a right-lateral slip component on fault F6.1 exposed in the east wall (Figures 12 and 13). Measurements of a piercing point on the cobble indicate less than 0.1 m of right-lateral oblique reverse slip on the fault with a 1.5:1 horizontal to vertical slip ratio. On the basis of the relatively small amount of displacement, we infer that earthquake A offset the cobble. If both earthquakes offset the cobble then we would expect a much greater amount of displacement that more closely agrees with the 0.6 m dip-slip component estimated by the cumulative displacement of the top of till along fault F6.1 produced by both earthquakes.

The deformation produced by both earthquakes A and B probably involved limited folding. Axial planes of oblate cobbles in the glacial till display remarkably consistent orientations across the entire trench and provide evidence for the absence of significant fold deformation. The cobble fabric is characterized by attitudes that dip 50° ± 20° toward the north as shown by stereonet projections of poles of the planes (Figure 11). Subtle folding produced by earthquakes, if any, was likely less than 20°. East-west-trending glacial striations in "bare-earth" LIDAR imagery suggest that ice overriding the till imprinted the cobble fabric (Figure 3a).

Like earthquake A, the most recent event failed to produce a surface scarp above faults exposed in the northern and southern parts of the trench of significant height to survive degradation by slope and forest soil processes. Ephemeral surface expressions of faulting also could easily be erased by grading and machinery used in logging activities during the early 20th century as is evident by the disturbed soils (unit 8) that overlie the faults. Even though trench evidence suggests two earthquakes produced slip across a broad zone of reverse and oblique-reverse faults, none of these signs explains the origin of the prominent scarp in LIDAR that motivated the investigation. The following discussion sketches alternative scenarios for the origin of the prominent scarp that defines the surficial expression of the Saddle Mountain West fault.

5.3 Did an Earthquake Produce the Surface Scarp?

The continuous expression of the surface scarp, so sharply defined by LIDAR for over 3 to 4 km, its impressive relief on the landscape (1 to 4 m high), and extensive faulting in trenches excavated across the scarp indicate an earthquake origin. But does the scarp at the Cargill Creek site reflect surface rupture during earthquake A or B, both events, or some other mechanism? Stratigraphic and structural data from directly below the scarp possess the best potential to evaluate this question. But conclusive evidence for earthquake deformation below the scarp is not revealed by the wedge-shaped, northward-thickening package of scarp colluvium (unit 5) that probably formed by a combination of graben-style surface rupture, soil upheaval by toppled tree roots and scarp modification by logging machinery.

Several stratigraphic clues provide conjectural evidence that development of the bowl-shaped depression in the till beneath the scarp (Figure 9) began as a graben caused by surface rupture during an earthquake. Like the graben examined in the southern part of the trench (Figure 10), the margins of the central depression coincide with faults, abundant fractures and open voids. Although it lacks clear signs of stratigraphic offset in massive till, fault F4 intersects the southern margin of the bowl and is the northern-most structure of a 1-m-wide zone of subvertical extensional fractures (Figure 9). Faults with similar orientations (F6, Figure 10) define the upslope side of the graben to the south. Open voids interconnected

by discontinuous fractures (F3, Figure 9) align below the northern margin of the bowl to form an inferred structure that drops unit 1b down to the south. Less than 0.2 m of vertical separation of the top of till across the bowl also is consistent with negligible vertical separation across the graben in the southern part of the trench. In both cases, faulting that produced the graben may have included a lateral component of slip.

Despite compelling signs of faulting along the margins of the depression, scarp colluvium of unit 5 probably was not derived from collapse and erosion of a scarp free face produced by fault rupture. If fault rupture alone explained the presence of the colluvial wedges, then unit 5b would bury a layer of older colluvium mantling the till (unit 3 or laterally adjacent colluvial deposits of similar age). The absence of older colluvium in the graben suggests it was removed. A different process exposed the scarp by completely excavating a concave depression down to glacial till. This hole was later filled from the south by units 5a and 5b that contain large till cobbles and boulders spalled from the scarp. A fault-generated graben would have vertically dropped preexisting deposits (e.g., unit 3) within a fault-bound block, and such deposits are absent in the depression. Tree throw, a common occurrence in temperate forests, could have created a hole by heaving colluvium bound in the root ball as the tree fell. However, examples of fallen Douglas fir trees near Price Lake expose flat root mats that formed in shallow soils above impermeable glacial till, not root balls. We believe that tree throw alone does not completely explain the origin of the depression and offer this alternative: If the shallow roots of a tree had penetrated deeper into soil down-dropped in an earthquake-related graben, then upheaval of the roots by tree throw could have removed pre-existing colluvium and exposed till in a deep hole bound by faults. What is not clear is whether this uprooting would remove all pre-existing deposits in the graben.

The remaining question: Why is the topographic scarp at the surface located above a buried depression? Discordance between the position of the surface scarp and the greatest amount of vertical offset on faults exposed in the trench suggests the scarp was modified by slope processes like tree throw and possibly logging activities. The largest vertical offset of the top of glacial till occurs to the north of the scarp where faults F1 and F2 accommodate 0.5 to 0.7 m of dip-slip displacement. As little as 0.1 to 0.2 m of net vertical displacement on the top of till occurs beneath the scarp. The presence of disturbed colluvium with abundant charcoal (unit 8) and anecdotal reports of an old skid road and a steam donkey that once operated near the site suggest that the scarp retreated several meters upslope due to erosion by heavy equipment.

6.0 SEISMIC HAZARDS OF THE SADDLE MOUNTAIN FAULT ZONE

6.1 Deformation Style

The bold expression of the Saddle Mountain West fault reflected by LIDAR surveys implies reverse dip-slip displacement, but competing geomorphic and structural evidence suggests a lateral component of slip that may meet or exceed the amount of reverse movement indicated by scarp height. In addition to clear geomorphic evidence for reverse slip, trench data reported here show apparent vertical offset of the contact between colluvium and till along steep reverse faults striking N60° to 80°E. Wilson (1975) and Wilson et al. (1979) documented reverse displacement on the West fault in a trench on the southern flank of Saddle Mountain showing Crescent Formation basalt thrust to the northwest over pre-Fraser till along a fault striking N19°E and dipping 67°SE.

Evidence for opposing lateral slip components comes from an offset cobble in the Cargill Creek trench identified by this study and striations on the surface of the Saddle Mountain East fault identified by Wilson et al. (1979). Reconstruction of a piercing point on the cobble indicates right-lateral oblique slip with a 1.5:1 horizontal to vertical slip ratio (see Structural Relations). Slickensides on the plane of the East fault, reported by Wilson et al. (1979), imply a left-lateral oblique slip component. These results are inconclusive in terms of the direction of lateral slip and other features cited as evidence for lateral slip only emphasize the ambiguity. For example, we noted both left- and right-lateral deflections along stream channels that crossed the Saddle Mountain East fault, but none allowed the deduction of an unequivocal sense of slip. Still more conflicting evidence includes interpreted dextral offset of a prominent magnetic anomaly north of Saddle Mountain identified by R. Blakely (personal communication, 2005). At the Canyon River fault in the southern Olympics, the postulated southwestern extension of the Saddle Mountain fault zone, trench data suggested a left-lateral slip component (Walsh et al., 1999; T. Walsh, personal communication, 2006).We conjecture that a significant change in strike along an oblique reverse fault (e.g., approximately 30°over the length of the West fault) may produce both dextral and sinistral lateral slip components depending on the slip azimuth and the regional strain field.

6.2 Deformation Rate and Slip Per Event

Estimating the amount of slip per earthquake and the slip rate of the Saddle Mountain West fault is difficult because slope processes (e.g., tree throw) have erased some evidence of surface rupture, 20th century timber harvesting has modified the scarp, and some deformation may have been accommodated by folding. In addition, because the fault scarp crosses a steep, timbered slope, the trench length was limited to 17 m and may not cross the entire deformation zone. We follow the approach of Nelson et al. (2003) to estimate the vertical component of displacement by summing stratigraphic offsets along faults and additional scarp growth, not accounted for by brittle deformation, attributed to folding. Folding may have accompanied faulting or occurred independently. We also estimate the possible right-lateral component of slip by assuming a 1.5:1 horizontal to vertical slip ratio. Table 7 lists the inferred amounts of fault slip per event, fold deformation, as well as vertical, horizontal and total slip rate estimates derived from trench data.

We place higher confidence on estimates of vertical deformation than on estimates of a possible right-lateral slip component. Faults that ruptured during the most recent earthquake (event B) show a total of about 0.8 m of vertical slip (Table 7). The discrepancy between offset strata measured in the trench, and additional deformation related to folding or unobserved faulting beyond the trench exposure amounts to about 0.4 m for a total vertical displacement estimate of about 1.2 m. Trench data suggest that less slip occurred during earthquake A with a total vertical component of about 0.5 m. Taken together, the total cumulative vertical displacement after both events, estimated from the height of the scarp, is 1.7 m. This

is a maximum estimate of vertical deformation because 20th century logging activities may have removed material from the base of the scarp. By comparison, Wilson et al. (1979) concluded that a 1.8-m-high buried scarp in basalt represented the vertical component of fault slip produced by two earthquakes evident in a trench on the southern flank of Saddle Mountain. Total cumulative displacement at this site, based on scarp height that reflects at least two events, is 3.9 m.

If earthquake B included a component of right-lateral slip, and assuming a horizontal to vertical slip ratio of 1.5:1, then about 1.8 m of dextral slip accompanied fault rupture (Table 7). Accounting for both the vertical and possible lateral components of slip amounts to a total slip estimate for earthquake B of 2.3 m. Despite several features in the trench that suggest a lateral slip component during event B, whether right-lateral slip accommodated this deformation remains uncertain. No clear evidence for lateral slip during earthquake A was identified.

The relatively brief length of the earthquake record (17 kyr) and sparse number of events results in a variation of slip rate estimates. The total vertical rate of deformation since the retreat of the Puget lobe of the Cordilleran ice sheet may exceed 0.1 m/kyr. Higher rates result when estimates consider only the deformation produced by the most recent earthquake (event B). Ignoring evidence of lateral slip, vertical deformation rates in the last 1.7 ka range from 0.7 to 1.2 m/kyr. If estimates include a right-lateral component of slip at a 1.5:1 horizontal to vertical slip ratio then total slip rate is 1.4 to 2.3 m/kyr.

6.3 Rupture Extent and Magnitude

Topographic expression related to surface rupture of the Saddle Mountain West fault extends 4 to 5 km from its southwestern limit near Dow Mountain to the eastern margin of Lilliwaup Swamp (Figure 3). LIDAR data available only to the south of Lilliwaup Swamp limits the evaluation of the total rupture length interpreted from fault-related geomorphology. However, aeromagnetic anomalies mapped by Blakely et al. (2005) suggest that an east-side-up structure coincident with the Saddle Mountain fault zone extends at least 18 km from Lake Cushman to the Hamma Hamma River. Once the most ephemeral features of surface rupture produced by earthquakes on the Saddle Mountain fault zone disappeared, only the most durable geomorphic features survived as short (<5 km), irregular and discontinuous scarps, similar to the complex patterns of surface rupture produced by historical reverse-fault earthquakes (Rubin, 1996; Kelson et al., 2001).

We use two approaches to estimate earthquake magnitude, (1) empirical relations between earthquake moment magnitude (M_w) and surface rupture length (Wells and Coppersmith, 1994); and (2) empirical relations between magnitude (M_w) and mean displacement that incorporates sampling statistics derived from slip distributions of historical earthquakes (Hemphill-Haley and Weldon, 1999). Following the Wells and Coppersmith (1994) approach, using the all-slip-type regression and assuming a total surface rupture length of 18 km yields a magnitude of M_w 6.5 ± 0.3. Although surface rupture length correlates closely with magnitude, using it in empirical regressions to estimate the size of prehistoric earthquakes born out by paleoseismic data is less reliable, as in this case, when the total length of coseismic surface rupture is in question. The second approach is more useful for quantifying uncertainties in magnitude estimates for this study because the regression includes mean displacement data that are best evaluated by paleoseismic investigations (Hemphill-Haley and Weldon, 1999). We use fault displacement data from the Cargill Creek trench (this study) and a trench across the West fault investigated by Wilson et al. (1979). Together, these sites probably span no more than about 10% to 15% of the total fault length (18 km). Assuming the 1.8-m-high buried fault scarp identified by Wilson et al. (1979) represents approximately equal slip (0.9 m) during two events, we calculate a mean displacement for the most recent earthquake of 0.85 m for two samples including the Cargill Creek site (Table 7). The magnitude calculated by this model, M_w 6.9 (-0.3, +0.9), exceeds the estimate using surface rupture length by almost half a magnitude point. A large earthquake (M_w 6.5 to 7) about 1,100 years ago also agrees with evidence

of fault-related flooding that drowned stumps now submerged below Price Lake (Hughes, 2005), an 18-km-long magnetic anomaly aligned with the Saddle Mountain fault zone (Blakely et al., 2005), and prehistoric rock avalanches in the southeastern Olympic Peninsula (Figure 1) attributed to strong earthquake shaking at about the same time (Bucknam et al., 1992).

7.0 CONCLUSIONS

Holocene displacement on the Saddle Mountain West fault, part of a system of oblique-reverse faults within the Saddle Mountain fault zone, was first identified by trench investigations in the 1970s by workers mapping the glacial stratigraphy of the southeastern Olympic Mountains (Carson, 1973; Carson and Wilson, 1974; Wilson, 1975; Wilson et al., 1979). Geomorphic expression of the West fault, first revealed by 1939 aerial photography flown after extensive clear cutting and more recently shown by LIDAR, includes a 4- to 5-km-long northeast trending, east-side-up scarp that extends from the northwestern flank of Dow Mountain on the south, across the Price Lake basin and Saddle Mountain, to Lilliwaup Swamp on the north (Figure 2). The objectives of the study included constructing a post-glacial earthquake chronology and assessing the rates and styles of deformation across the Saddle Mountain fault zone as inputs for regional strain models and hazard maps for western Washington.

To accomplish these objectives, we investigated a trench across the West fault at Cargill Creek where a single, 1- to 2-m high scarp deforms Vashon glacial till and outwash and post-glacial colluvial deposits (Figure 3). Northeast-striking primary faults and fractures dipping 55° to 80° southeast and secondary fractures with similar strikes but dipping 50° to 55° north characterized a 10-m-wide zone of deformation exposed in the trench. Interpretations of stratigraphic and structural relations imply two earthquakes with a cumulative vertical component of fault displacement of about 1 m. The total height of the scarp (1.7 m) suggests additional deformation was accommodated by folding or on ancillary faults located outside the 17-m-long trench exposure. However, the consistent northward dip of cobbles cemented in till throughout the trench suggest that tilting caused by folding did not exceed 20°. Right-lateral oblique reverse displacement of a cobble firmly cemented in till provides the only clue to evaluate possible lateral component of slip and suggests a 1.5:1 horizontal to vertical slip ratio.

Trench data provided constraints on when the earthquakes occurred, slip per event and post-glacial slip rate estimates, and the probable earthquake magnitude that produced the most recent ground rupture. The first occurred between 17 and 8.5 ka based on the onset of ice retreat in the Puget Lowland and ^{14}C ages on detrital charcoal. ^{14}C age on detrital charcoal limit the timing of the most recent event to after 1.7 ka, but we infer that this earthquake is the same event that produced surface rupture that submerged a spruce forest below Price Lake between 1,000 and 1,300 cal yr BP (Hughes, 2005). The total vertical deformation rate is ~0.1 m/kyr for two events in the past 17 ka, whereas, rates of vertical deformation since the most recent earthquake range from 0.7 to 1.2 m/kyr. Displacements of the contact between colluvium and glacial till indicate 0.2 to 0.8 m of vertical slip per earthquake. Using both empirical relations between magnitude and surface rupture length (Wells and Coppersmith, 1994) and regressions on magnitude and mean displacement that incorporate statistics on historical earthquake slip distributions Hemphill-Haley and Weldon, 1999) places the size of the most recent earthquake on the Saddle Mountain fault zone at M_w 6.5 to 7.

8.0 ACKNOWLEDGEMENTS

We thank B. Sherrod for the many dialogs that encouraged us to pursue this project and for assistance with LIDAR data and property access. J. Kvalle of the Washington Department of Natural Resources facilitated permitting, logistics and provided important local information. We acknowledge preliminary data from related USGS field studies of Price Lake shared by J. Hughes and R. Blakely and consequent stimulating discussions. Professor R. Carson and his industrious students M. Zeliff and C. Iacoboni of Whitman College provided considerable assistance with the interpretation and description of geologic units, logistical tasks in the trench and completed the coring transect across the scarp. For her senior thesis, Zeliff developed an interpretation of the stratigraphic profile along the transect. H. Kelsey interpreted soil stratigraphy in the trench. Ray Witter assisted with trenching and the coring transect. The following workers provided critical insight during a field peer review of the trench that helped us formulate our interpretations: R. Haugerud, A. Nelson, S. Personius, E. Schermer, T. Walsh, R. Wells. Carolyn Mosher employed meticulous care developing the graphics. StereoWin 1.2 was used for stereographic analysis of cobble measurements.

9.0 REFERENCES

Atwater, B.F., and Moore, A.L., 1992, A tsunami about 1,000 years ago in Puget Sound, Washington: Science, 258, 1614-1617.

Blakely, R.J., Wells, R.E., and Weaver, C.S., 1999, Puget Sound Aeromagnetic maps and data: U.S. Geological Survey, Open-File Report OF-99-514, scale 1:100,000.

Blakely, R.J., Wells, R.E., Weaver, C.S., and Johnson, S.Y., 2002, Location, structure and seismicity of the Seattle fault zone, Washington: Evidence from aeromagnetic anomalies, geologic mapping and seismic reflection data: Geological Society of America Bulletin, 114, 167-177.

Blakely, R.J., J.F. Hughes, B.L. Sherrod, and R.E. Wells, 2005, Hunting the Saddle Mountain fault zone in the Olympic Peninsula with airplane and canoe: Eos Transactions AGU, 86 (52), Fall Meeting Supplement, Abstract, S51C-1021.

Booth, D.B., 1994, Glociofluvial infilling and scour of the Puget Lowland, Washington, during ice-sheet glaciation: Geology, v. 22, p. 695-698.

Booth, D.B., Troost, K.G., Clague, J.J., and Waitt, R.B., 2004, The Cordilleran ice sheet, *in* Ehlers, J. and Gibbard, P.L., eds., Quaternary Glaciations—Extent and Chronology, Part II: North America, Elsevier, p. 17-43.

Brandon, M.T., Roden-Tice, M.K., and Garver, J.I., 1998, Late Cenozoic exhumation of the Cascadia accretionary wedge in the Olympic Mountains, northwest Washington State: Geological Society of America Bulletin, v. 110, p. 985-1009.

Brocher, T.M., Parsons, T., Blakely, R.J., Christensen, N.I., Fisher, M.A., Wells, R.E., and the SHIPS working group, 2001, Upper crustal structure in Puget Lowland, Washington: Results from the 1998 seismic hazard investigation in Puget Sound: Journal of Geophysical Research, 106, 13,541-13,564.

Bucknam, R.C., Hemphill-Haley, E., and Leopold, E.B., 1992, Abrupt uplift within the past 1,700 years at southern Puget Sound, Washington: Science, v. 258, p. 1611-1614.

Carson, R.J., 1970, Quaternary geology of the south-central Olympic Peninsula, Washington, University of Washington, Ph.D. dissertation, 67 p.

Carson, R.J., 1973, First known active fault in Washington: Washington Geologic Newsletter, Washington Division of Geology and Earth Resources, v. 1, no. 3, p. 1-2.

Carson, R.J., 1976, Preliminary geologic map of north-central Mason County, Washington: Washington Division of Geology and Earth Resources Open-File Report 76-2, scale 1:62,500.

Carson, R.J., and J.R. Wilson, 1974, Quaternary faulting on Dow Mountain, Mason County: Washington Geologic Newsletter, Washington Division of Geology and Earth Resources, v. 2, no. 4, p. 1.

Easterbrook, D.J., 1986, Stratigraphy and chronology of Quaternary deposits of the Puget Lowland and Olympic Mountains of Washington and the Cascade Mountains of Washington and Oregon, *in* Sibrava, V., Bowen, D.Q., and Richmond, G.M., eds., Quaternary Science Reviews, v. 5, p. 145-159.

Flück, P., Hyndman, R.D., and Wang, K., 1997, Three-dimensional dislocation model for great earthquake of the Cascadia subduction zone: Journal of Geophysical Research, v. 102, p. 20,539-20,550.

Gower, H.D., Yount, J.C., and Crosson, R.S., 1985, Seismotectonic map of the Puget Sound region, Washington: U.S. Geological Survey, Miscellaneous Investigations Series Map I-1613, scale 1:250000.

Haugerud, R.A., D.J. Harding, S.Y. Johnson, J.L. Harless and C.S. Weaver, 2003, High-resolution LIDAR topography of the Puget Lowland, Washington—A bonanza for Earth science: GSA Today, v. 13, no. 6, p. 4-10.

Hemphill-Haley, M.A. and Weldon, R.J., 1999, Estimating prehistoric earthquake magnitude from point measurements of surface rupture, Bulletin of the Seismological Society of America, v. 89, n. 5, p. 1264-1279.

Hughes, J.F., 2005, Meters of synchronous Holocene slip on two strands of a fault in the western Puget Sound Lowland, Washington: Eos Transactions AGU, 86 (52), Fall Meeting Supplement, Abstract S51C-1020.

Johnson, S.Y., Potter, C.J., and Armentrout, J.M., 1994, Origin and evolution of the Seattle fault and Seattle basin: Geology, v. 22, p. 71-74.

Johnson, S.Y., Dadisman, S.V., Childs, J.R., and Stanley, W.D., 1999, Active tectonics of the Seattle Fault and central Puget Sound, Washington—Implications for earthquake hazards: Geological Society of America Bulletin, 108, 334-354.

Johnson, S.Y., and 9 others, 2003, Evidence for one or two late Holocene earthquakes on the Utsalady Point fault, northern Puget Lowland, Washington: Geological Society of America Abstracts with Programs, v. 35, n. 6, p. 479.

Kelson, K.I., Kang, K.-H., Page, W.D., Lee, C.-T., and Cluff, L.S., 2001, Representative styles of deformation along the Chelungpu fault from the 1999 Chi-Chi (Taiwan) earthquake: Geomorphic characteristics and responses of man-made structures: Seismological Society of America Bulletin, 91, 930-952.

Lewis, J.C., Unruh, J.R., and Twiss, R.J., 2003, Seismogenic strain and motion of the Oregon coast block: Geology, v. 31, p. 183-186.

McCalpin, J.P., 1998, Paleoseismology: Orlando, Florida: Academic Press, 608 p.

Khazaradze, G., Qamar, A., and Dragert, H., 1999, Tectonic deformation in western Washington from continuous GPS measurements: Geophysical Research Letters, 26, 3153-3156.

Miller, M.M., Johnson, D.J., Rubin, C.M., Dragert, H., Wang, K., Qamar, A., and Goldfinger, C., 2001, GPS-determination of along-strike variation in Cascadia margin kinematics: Implications for relative plate motion, subduction zone coupling and permanent deformation: Tectonics, 20, 161-176.

Nelson, A.R., Johnson, S.Y., Wells, R.E., Pezzopane, S.K., Kelsey, H.M., Sherrod, B.L., Bradley, L.A., Koehler, R.D., Bucknam, R.C., Haugerud, R.A., and LaPrade, W.T., 2002, Field and laboratory data from an earthquake history study of the Toe Jam Hill fault, Bainbridge Island, Washington: U.S. Geological Survey Open-File Report 02-60, 2 plates and 37 p. text.

Nelson, A.R., Johnson, S.Y., Wells, R.E., Kelsey, H.M., Sherrod, B.L., Pezzopane, S.K., Bradley, L., and Koehler, R.D., 2003, Earthquake history of the Toe Jam Hill fault, Bainbridge Island, Washington: Geological Society of America Bulletin, accepted.

Ness, A.O., and Fowler, R.H., 1960, Soil Survey of Mason County, Washington, Soil Conservation Service: U.S. Department of Agriculture, Online soil survey available at: http://soils.usda.gov/

Peterson, M.D., Cramer, C.H., and Frankel, A.D., 2002, Simulations of seismic hazard for the Pacific Northwest of the United States from earthquakes associated with the Cascadia subduction zone: Pure and Applied Geophysics, v. 159, p. 2147-2168.

Porter, S. C., and Swanson, T. W., 1998, Radiocarbon age constraints on rates of advance and retreat of the Puget lobe of the Cordilleran ice sheet during the last glaciation: Quaternary Research, v. 50, p. 205-213.

Pratt, T.L., Johnson, S., Potter, W., Stephenson, W., and Finn, C., 1997, Seismic reflection images beneath Puget Sound western Washington state: The Puget Lowland thrust sheet hypothesis: Journal of Geophysical Research, v. 102, p. 27,469-27,489.

Reimer, P.J., M.G.L. Baillie, E. Bard, A. Bayliss, J.W. Beck, C. Bertrand, P.G. Blackwell, C.E. Buck, G. Burr, K.B. Cutler, P.E. Damon, R.L. Edwards, R.G. Fairbanks, M. Friedrich, T.P. Guilderson, K.A. Hughen, B. Kromer, F.G. McCormac, S. Manning, C. Bronk Ramsey, R.W. Reimer, S. Remmele, J.R. Southon, M. Stuiver, S. Talamo, F.W. Taylor, J. van der Plicht, and C.E. Weyhenmeyer, 2004, Radiocarbon 46:1029-1058.

Rubin, C.M., 1996, Systematic underestimation of earthquake magnitudes from large intracontinental reverse faults: Historical ruptures break across segment boundaries: Geology, 24, 989-992.

Schoeneberger, P.J., Wysocki, D.A., Benham, E.C., and Broderson, W.D.(editors), 2002. Field book for describing and sampling soils, Version 2.0. Natural Resources Conservation Service, National Soil Survey Center Lincoln, NE.

Schuster, R.L., Logan, R.L., and Pringle, P.T., 1992, Prehistoric rock avalanches in the Olympic Mountains, Washington: Science, v. 258, p. 1620-1621.

Sherrod, B.L., Bucknam, R.C., and Leopold, E.B., 2000, Holocene relative sea level change along the Seattle fault at Restoration Point, Washington: Quaternary Research, v. 54, p. 384-393.

Sherrod, B.L., 2001, Evidence for earthquake-induced subsidence about 1,100years ago in coastal marshes of southern Puget Sound, Washington: Geological Society of America Bulletin, 113, 1299-1311.

Sherrod, B.L., T.M. Brocher, C.S. Weaver, R.C. Bucknam, R.J. Blakely, H.M. Kelsey, A.R. Nelson, R. Haugerud, 2004, Holocene fault scarps near Tacoma, Washington, USA: Geology, v. 32, p. 9-12.

Stuiver, M., and Reimer, P.J., 1993, Radiocarbon, 35, 215-230.

Tabor, R. W.; Cady, W. M., 1978, Geologic map of the Olympic Peninsula, Washington: U.S. Geological Survey Miscellaneous Investigations Series Map I-994, 2 sheets, scale 1:125,000.

Walsh, T.J., Logan, R.L., Neal, K.G., and Palmer, S.P., 1999, Active fault investigations on the Canyon River fault, southern Olympic Range, Washington: Final Technical Report, U.S. Geological Survey, National Earthquake Hazards Reduction Program, 20 p.

Wells, R.E., Weaver, C.S., Blakely, R.J., 1998, Fore-arc migration in Cascadia and its neotectonic significance: Geology, v. 26, p. 759-762.

Wilson, J.R., 1975, Geology of the Price Lake area, Mason County, Washington: Raleigh, North Carolina State University, M.S. thesis, 79 p.

Wilson, J.R., Bartholomew, M.J., and Carson, R.J., 1979, Late Quaternary faults and their relationship to tectonism in the Olympic Peninsula: Washington, Geology, v. 7, p. 235-239.

TABLES

Table 1. Descriptive information for geologic units in Cargill Creek trench

Unit No.	Station (m)		Matrix Texture (sand, silt, clay)	Coarse Fraction				Matrix Color (dry)		Moisture	Field Density	Soil Characteristics			Interpretation
	Horizontal	Vertical		Pebbles	Cobbles	Boulders	Angularity	Matrix	Mottles			Horizon	Structure	Roots	
1a	8.35	2.67	Sandy loam (70, >25, <5)	40-45	5	0	Rounded to subrounded	Olive brown (2.5Y4/4)	0	Damp	Dense	C	msv	1 vf-f C-R	Overconsolidated ice contact drift
1b	7.89	2.14	Sandy loam (65, 30, <5)	55-60	5	<1	Subangular to subrounded	Dark olive brown (2.5Y3/3)	Dark yellowish brown (10YR3/4)	Damp	Loose	C	0-1 vf-f sbk	1 vf-c random	Overconsolidated ice contact drift
1cCox	nd	nd	Sand (85, >10, <5)	65-70	5-10	<1	nd	Dark yellowish brown (10YR3/6 moist)	0	Damp	Dense	2Cox1	2-3 c-vc pl	1 vf vertical	Glacial drift impregnated with translocated, oxidized silt
1dCox	nd	nd	Sand (90, <10, <1)	65-70	5-10	0	nd	Very dark grayish brown (10YR3/2 moist)	0	Damp	Dense	2Cox2	0-1 f-m bk	0-1 vf vertical	Strongly cemented glacial drift
2a	13.88	5.86	Sandy loam (65, 35, 0)	40-45	<5	0	Rounded to subrounded	Yellowish brown (10YR5/8)	0	Damp	Loose	1Cox2	0-1 vf-f gr	1 vf, 2 m random	Stratified glacial outwash or ablation till
2b	13.88	5.95	Loamy sand (nd)	75-80	5-10	0	Subangular to subrounded	Grayish brown (2.5y5/2	Yellowish brown (10YR 5/8	Damp	Loose	1Cox2	sg	0	Stratified glacial outwash or ablation till
2c	13.88	6.08	Silt (15, 85, <1)	60-70	0	0	Rounded to subrounded	Dark yellowish brown (10YR4/6) Strong brown (7.5YR4/6)	0	Damp	Loose	1Cox2	msv	1 vf-c random	Stratified glacial outwash or ablation till
3aCox	12.92	5.92	Loamy sand (75, 25, <1)	75-80	<5	0	Rounded to subangular	Yellowish brown (10YR5/6)	0	Damp	Loose	1Cox1	sg	2 vf vertical 1 f, 1 m, 2 c random	Colluvium derived from units 1 and 2
3bBC	12.97	6.13	Sandy loam (50, 50, <1)	50	<2	0	Subangular to subrounded	Dark yellowish brown (10YR4/6)	0	Damp	Loose	BC	1 f-m sbk	1 vf-f random, 1 m-c, 2 vc horizontal	Colluvium derived from units 1 and 2
3cBw	13.64	6.5	Loamy sand (80, 20, <1)	60-65	<5	0	Rounded	Dark yellowish brown (10YR4/6)	0	Damp	Loose	Bw	1 f-m sbk	1 vf-f random, 1 m-c, 2 vc horizontal	Colluvium derived from units 1 and 2

Unit No.	Station (m)		Matrix Texture (sand, silt, clay)	Coarse Fraction				Matrix Color (dry)		Moisture	Field Density	Soil Characteristics			Interpretation
	Horizontal	Vertical		Pebbles	Cobbles	Boulders	Angularity	Matrix	Mottles			Horizon	Structure	Roots	
4a	6.31	2.37	Silt loam (35, 65, <1)	30-35	15-20	0	Subangular to subrounded	Dark yellowish brown (10YR4/6	0	Dry	Loose	nd	msv	2 vf-f, 1 m random	Colluvium in fault contact with unit 1
4bBw	2.41	1.12	Silt loam (25, 75, <1)	40-45	5-10	<1	Rounded to subrounded	Yellowish brown (10YR5/8)	0	Damp to dry	Loose	Bw	1 vf-f sbk	2 vf, 1 f, 1 m-vc random	Colluvium derived from units 1, 2 and 3
4bBw	8.48	3.66	Silt loam (40, 60, <1)	35-40	5	0	Rounded to subangular	Dark yellowish brown (10YR4/6)	0	Damp	Loose	Bw	0-1 vf sbk	1 vf-f, 2 m, 1 c, 2 vc random	Colluvium derived from units 1, 2 and 3
4cBwb	3.15	0.9	Silt loam (25, 70 <5)	35-40	<5	0		Brown (7.5YR4/4)	0	Damp	Loose	Bwb	1-2 m sbk	nd	Buried Bw horizon develoed ingravelly silt
4dAB	4.65	1.9	Silt (15, 85, <1)	30-35	10-15	<2	Rounded to subangular	Dark yellowish brown (10YR4/6)	0	Damp to dry	Loose	AB	msv	3 f-vf, 2 m, 1 c random	AB soil horizon developed in colluvium
5a	10.4	3.63	Loamy sand (70, 30, <1)	50-55	20-25	0	Subangular to subrounded	Gray (10YR5/1); Brownish yellow (10YR6/6)	0	Dry to damp	Loose	nd	msv	1 vf-m, 2 c, 1vc random	Scarp colluvium derived predominantly from unit 1
5b	9.5	3.52	Sandy loam (65, 35, <1)	55-65	15-25	0	Angular to subrounded	Yellowish brown (10YR5/6)	0	Dry	Loose	nd	msv	3 vf-f, 2 m-c random	Scarp colluvium derived predominantly from unit 3 with conspicuous cobble-sized blocks of unit 1
6a	9	3.57	Sand (95, 5, <1)	40-50	40-50	0	Subangular to subrounded	Gray (10YR5/1)	0	Dry to damp	Loose	nd	msv	2 vf, 1f random	Colluvium
6b	8.45	3.74	Silt loam (30, 70, <1)	35-40	5-10	0	Subrounded	Olive brown (2.5Y4/4)	0	Dry	Loose	nd	0-1 f sbk	1 vf-c, 2 vc random	Colluvium
6cBw	8.8	3.8	Sandy loam (65, 35, <1)	45-50	5	0	Subrounded	Dark yellowish brown (10YR3/4)	0	Damp	Loose	Bw	msv	1 vf-m random	Colluvium
7a	4.1	1.8	Silt loam (25, 75, <1)	35-40	5-10	0	Rounded to subangular	Dark yellowish brown (10YR3/6)	0	Damp to dry	Loose	nd	1 f-m sbk	2 vf-f, 1 m random	Colluvium filling tree throw crater
7bAO	4.2	2.03	Silt (5, 95, <1)	5-10	15-20	0	Rounded to subangular	Black (10YR2/1)	0	Damp to dry	Loose	AOb	msv	3 vf-f, 1 m-c random	Buried AO horizon

Unit No.	Station (m)		Matrix Texture (sand, silt, clay)	Coarse Fraction				Matrix Color (dry)		Moisture	Field Density	Soil Characteristics			Interpretation
	Horizontal	Vertical		Pebbles	Cobbles	Boulders	Angularity	Matrix	Mottles			Horizon	Structure	Roots	
8aAb	4.36	2.16	Silt (5, 95, <1)	40-45	5	0	Subangular to subrounded	Dark yellowish brown (10YR4/4)	0	Damp to dry	Loose	Ab	0-1 f gr	3 vf, 1 f-c	Buried A horizon developed in colluvium
8b	9.79	4.1	Loamy sand (80, 20, <1)	35-40	20-25	0	Subrounded to rounded	Very dark brown (10YR2/2)	0	Dry	Loose	nd	msv	3 vf-m, 1 c-vc random	Colluvium, with abundant charcoal
8c	10.2	5.36	Loamy sand (75, 25, <1)	40-45	15-20	0	Subangular to subrounded	Dark yellowish brown (10YR4/4)	0	Dry	Loose	nd	msv	2 vf-f, 1 m-vc random	Colluvium
9aA/O	16.2	7.74	Silt (5, 95, <2)	5-10	20-25	0	Subangular to subrounded	Very dark brown (10YR2/2 to 7.5YR2.5/3)	0	Damp to dry	Loose	A/O	1 vf sbk	3 vf-f random, 2 m, 1 c horizontal	Organic litter and forest soil developed in unit 3
9bO	10.17	4.77	Silt loam (45, 55, <1)	20-25	5-10	0	Rounded	Black (10YR2/1)	0	Damp to dry	Loose	O	msv	3 vf-c random	Modern O horizon
9cO	3.66	2.02	Silt loam (50, 50, <1)	5-10	<2	0	Subangular to subrounded	Black (7.5YR2.5/1)	0	Damp	Loose	O	msv	3 vf-c random	Modern O horizon impacted by 20th Century logging

Table 2. Pebble and cobble lithologies from glacial drift exposed in Cargill Creek trench compared to Puget and Alpine drift.

Pebble/Cobble Lithology	Percent Composition		
	Cargill Creek	Puget Drift	Alpine Drift
Sandstone (mostly greywacke)	28	22	36
Basalt	50	26	27
Diabase and gabbro	3	12	17
Chert and jasper	3	9	3
Shale, argillite, and slate	0	2	2
Granite and granodiorite	1	7	0
Quartz and quartzite	1	3	0
Diorite	2	3	0
Rhyolite and dacite	2	0	0
Other*	10	16	15

*Includes andesite, gneiss, epidote, conglomerate, Tertiary sedimentary rock, and undetermined lithologies.
Note: Clast lithologies at Cargill Creek identified by Professor Robert J. Carson from counting 100 pebbles and cobbles. Percent compositions for Puget and Alpine drift from south-central Olympic Peninsula from Carson (1970).

Table 3. Field description of soil profile, west wall of Cargill Creek trench

Depth Interval (cm)	Horizon	Parent Material	Geologic Unit	Matrix Texture (sand, silt, clay)	Coarse Fraction (Percent Area)	Munsell Color, Moist	Structure	Roots	Boundary
0-7	O	Forest litter	20d	Predominantly organics	nd	nd	Root mat	3 vf-f random, 2m, 1 c horizontal	Diffuse, wavy
7-22	A	Colluvium	20d	Silt (30, 70, 0)	55-65	Very dark brown (10YR2/2)	1 vf-f sbk	3 vf-f random, 2m, 1 c horizontal	Gradual, wavy
22-46	Bw	Colluvium	20c	Sandy loam (50, 45, <5)	55-65	Strong Brown (7.5YR4/6)	1 f-m sbk	2 vf-f random, 1 m-c horizontal	Diffuse, wavy
46-73	BC	Colluvium	20b	Silt loam (35, 60, 5)	55-65	Strong Brown (7.5YR4/6)	1 f-m sbk	2 vf-f random, 1 m-c horizontal	Diffuse, wavy
73-82	1Cox	Colluvium	20a	Sand (85, 15, 0)	55-65	Very dark grayish brown (10YR3/2)	sg	1 vf vertical	Clear, smooth
82-94	2Cox1	Glacial till	1dCox1	Sand (80, 15, 5)	70-80	Dark yellowish brown (10YR3/6)	2-3 c-vc pl	1 vf vertical	Clear to gradual, smooth
94-109	2Cox2	Glacial till	1cCox2	Sand (90, 10, <1)	70-80	Very dark grayish brown (10YR3/2)	1 f-m bk	0-1 vf vertical	Clear, wavy
109-144	2C	Glacial till	1a	Sand (95, 5, 0)	70-80	Very dark grayish brown (10YR3/2)	msv	0-1 vf vertical	Nd

Table 4. Mean pole calculations and 95% confidence intervals for measured clast orientations in glacial till grouped by trench section.

Trench section (meters)	No. of clasts	Mean pole		95% confidence (degrees)
		Trend	Plunge	
1-5	15	208.5	54.4	17.3
5-7.5	23	176.7	49.9	16.5*
7.5-10	22	183.2	47.6	15.6*
10-13	11	174.3	51.9	16.6
13-17	18	181.5	47	18.3*
1-17 (total)	89	184	50.3	7.4

*Confidence cones not reliable

Table 5. Radiocarbon isotopic analysis results for detrital charcoal sampled from the Cargill Creek trench, Saddle Mountain West fault.

Lab Number	Sample Name	Sample Coordinates (x, y in meters)	Sample Provenance	Material Dated	$\delta^{13}C$	Lab-reported Age (^{14}C yr BP at 1σ)	Calibrated age (cal yr BP at 2σ)
32081	PL05RC-10	6.53, 2.67	4bBw (colluvium)	charcoal	-25.1	1020 ± 35	800-1050
32079	PL05RC-4	6.22, 2.46	4bBw (colluvium)	charcoal	-22.7	1390 ± 50	1180-1390
32082	PL05RC-15	10.42, 4.25	5b (colluvium)	charcoal	-26.1	1550 ± 40	1360-1530
32080	PL05RC-6	6.17, 2.27	4a (colluvium)	charcoal	-26.7	1760 ± 40	1560-1810
32084	PL05RC-18	14.9, 6.82	3cBw (colluvium)	charcoal	-23.1	1820 ± 35	1630-1860
32083	PL05RC-16	11.62, 5.34	3aCox (colluvium)	charcoal	-23.1	7650 ± 50	8380-8540

Table 6. Radiocarbon isotopic analysis results for detrital plant macrofossils sampled from sediment cores across Saddle Mountain West fault.

Lab Number	Core Number	Sample Depth in Core (m)	Sample Provenance	Material Dated	$\delta^{13}C$	Lab-reported Age (^{14}C yr BP at 1σ)	Calibrated age (cal yr BP at 2σ)
32248	PL05C1	2.60	Buried peat layer	peat	-30.0	7380 ± 50	8040-8330
32249	PL05D3	3.32	Buried peat layer	seeds	-27.8	7720 ± 50	8420-8590

Table 7. Fault Displacement, Fold Deformation and Slip Rate Estimates From the Cargill Creek Trench, Saddle Mountain West Fault

Surface Faulting Event(s)[1]	Vertical Fault Slip Per Event(s) (m)[2]	Additional Vertical Deformation (m)[3]	Cumulative Displacement			Age of Stratigraphic Datum (ka)[7]	Slip Rate Estimates		
			Vertical Component (m)[4]	Right-lateral Component (m)[5]	Total Slip (m)[6]		Vertical Deformation Rate (m/kyr)[8]	Horizontal Slip Rate (m/kyr)[9]	Total Slip Rate (m/kyr)[10]
Event B	0.8 (0.5-1.0)	0.4 (0-0.7)	1.2 (0.5-1.7)	1.8 (0-2.6)	2.3 (0.6-3.2)	1.7-1.0	0.7-1.2	1.1-1.6	1.4-2.3
Event A	0.2 (0-0.5)	0.3 (0-0.4)	1.7 (0.5-1.7)	nd	nd	16.7-17	>0.1	nd	nd
West fault trench	1.8 (two events)	2.1	3.9	nd	nd	Salmon Springs till[11]	0.004	nd	nd

Notes: Range of uncertainty shown in parentheses; nd, no data.
[1]Earthquakes A and B interpreted from Cargill Creek trench data (this study). West fault trench data from Wilson et al. (1979).
[2]Inferred vertical displacement per event estimated by summing offsets of strata measured across faults.
[3]The balance of vertical deformation constituting the difference between measured offset of strata and far-field scarp height. Deformation may be due to folding or faulting beyond the area investigated by trenching.
[4]The sum of columns 2 and 3.
[5]Possible right-lateral slip component assuming a 1.5:1 horizontal to vertical slip ratio.
[6]Total possible slip calculated assuming a fault dip of 60°.
[7]Estimated age of offset strata in thousand years B.P. (ka) from Plate 1 and Table 5. Event B timing constrained by detrital charcoal ages from the trench and ages from drowned stumps rooted in a buried soil beneath Price Lake (Hughes, 2005). Event A occurred after initial retreat of glacial ice about 17 ka (Porter and Swanson, 1998).
[8]Calculated in meters per thousand years (m/kyr) by dividing column 4 by column 7.
[9]Calculated by dividing column 5 by column 7.
[10]Calculated by dividing column 6 by column 7.
[11]The estimated age of pre-Fraser till, recognized as Salmon Springs till by Wilson (1975), is 1,000 ka (Booth et al., 2004).

FIGURES

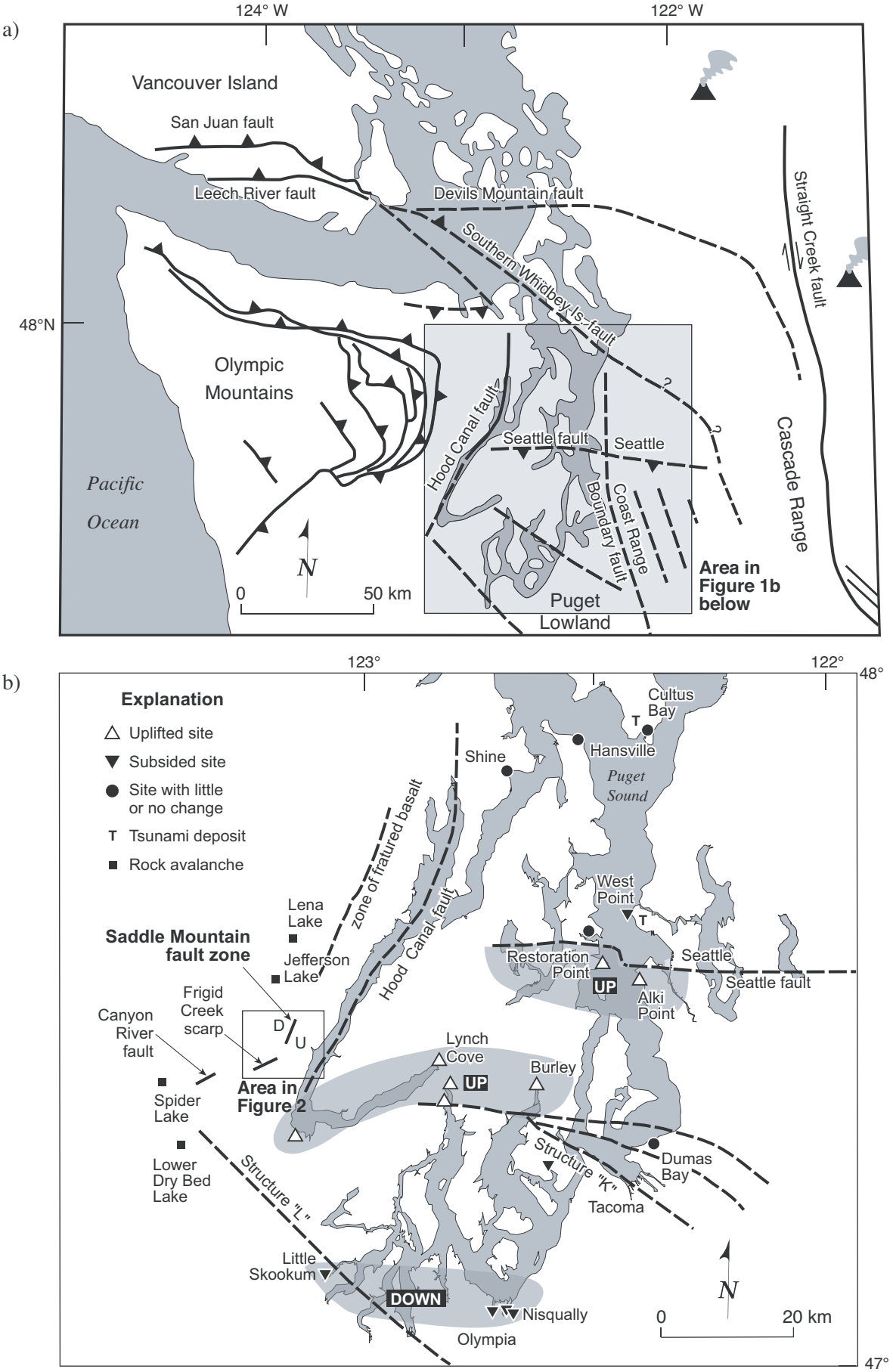

Figure 1. (a) Tectonic map of western Washington (modified from Johnson et al., 1999) showing crustal faults in the Puget Lowland bound by the Olympic and Cascade Mountain ranges. (b) Map showing regions of tectonic uplift and subsidence, tsunami deposits, and rock avalanches in the Puget Lowland that occurred about 1,100 years ago (modified from Sherrod, 2001; Bucknam et al., 1992; Atwater and Moore, 1992). Fault locations from Johnson et al. (1999), Gower et al. (1985), and unpublished data of Sherrod (pers. comm. 2003).

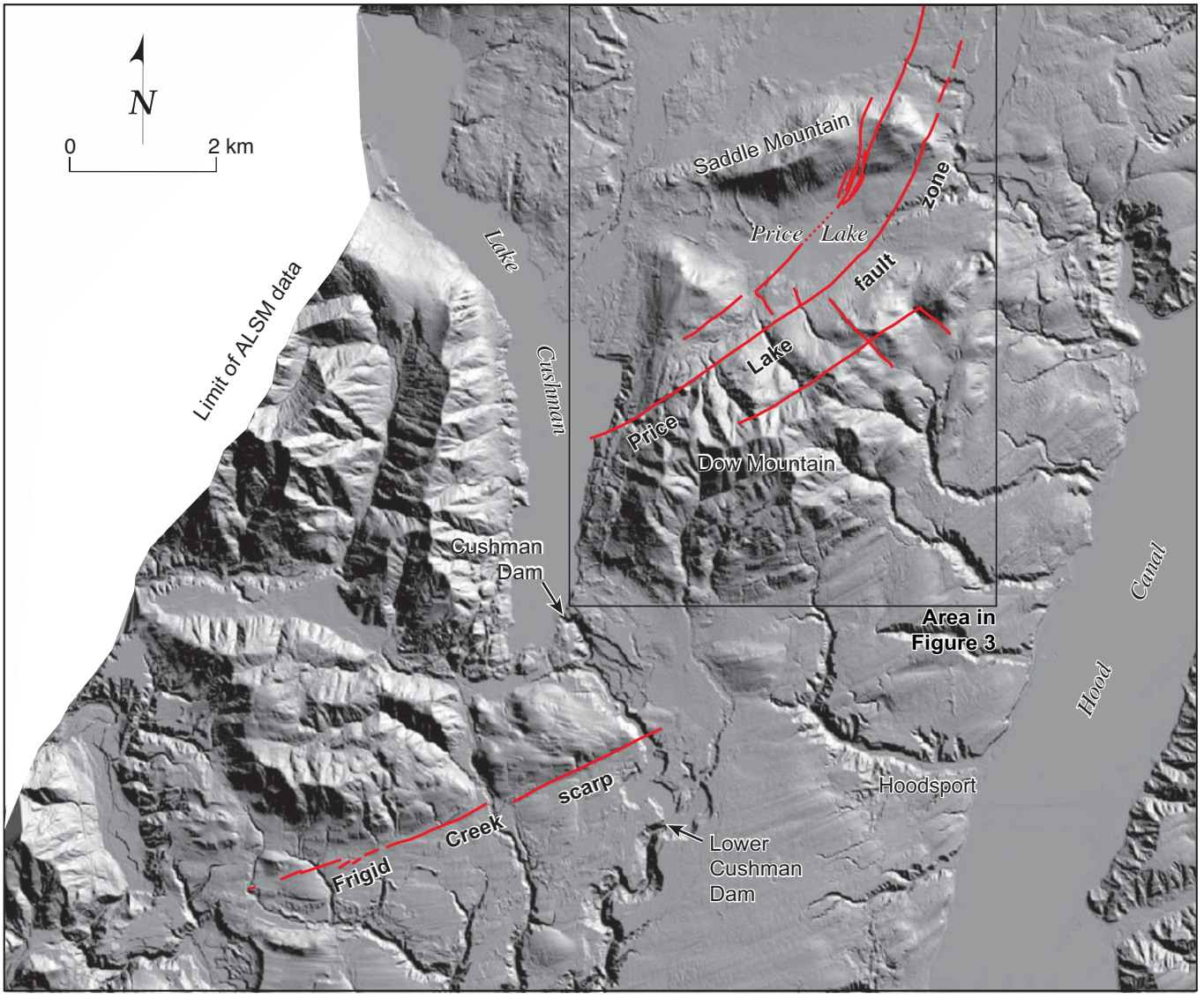

Figure 2. Light detection and ranging (lidar) image of the southeastern Olympic Peninsula near Hoodsport, Mason County, Washington showing northwest-facing scarps of the Saddle Mountain fault zone and recently identified southeast-facing scarps near Frigid Creek. The Saddle Mountain fault zone consists of two to three northeast-striking reverse faults that traverse across the northern flank of Dow Mountain, through Price Lake to the northeast and bisect Saddle Mountain. Several northwest-trending topographic scarps and lineaments intersect the northeast-striking faults suggesting that the fault zone may consist of a series of imbricated reverse faults and perpendicular tear faults. Previous study of the Saddle Mountain faults by Wilson et al. (1979) reported evidence for latest-Pleistocene and Holocene displacement. For a detailed lidar image and corresponding geologic map of the Saddle Mountain fault zone see Figure 3.

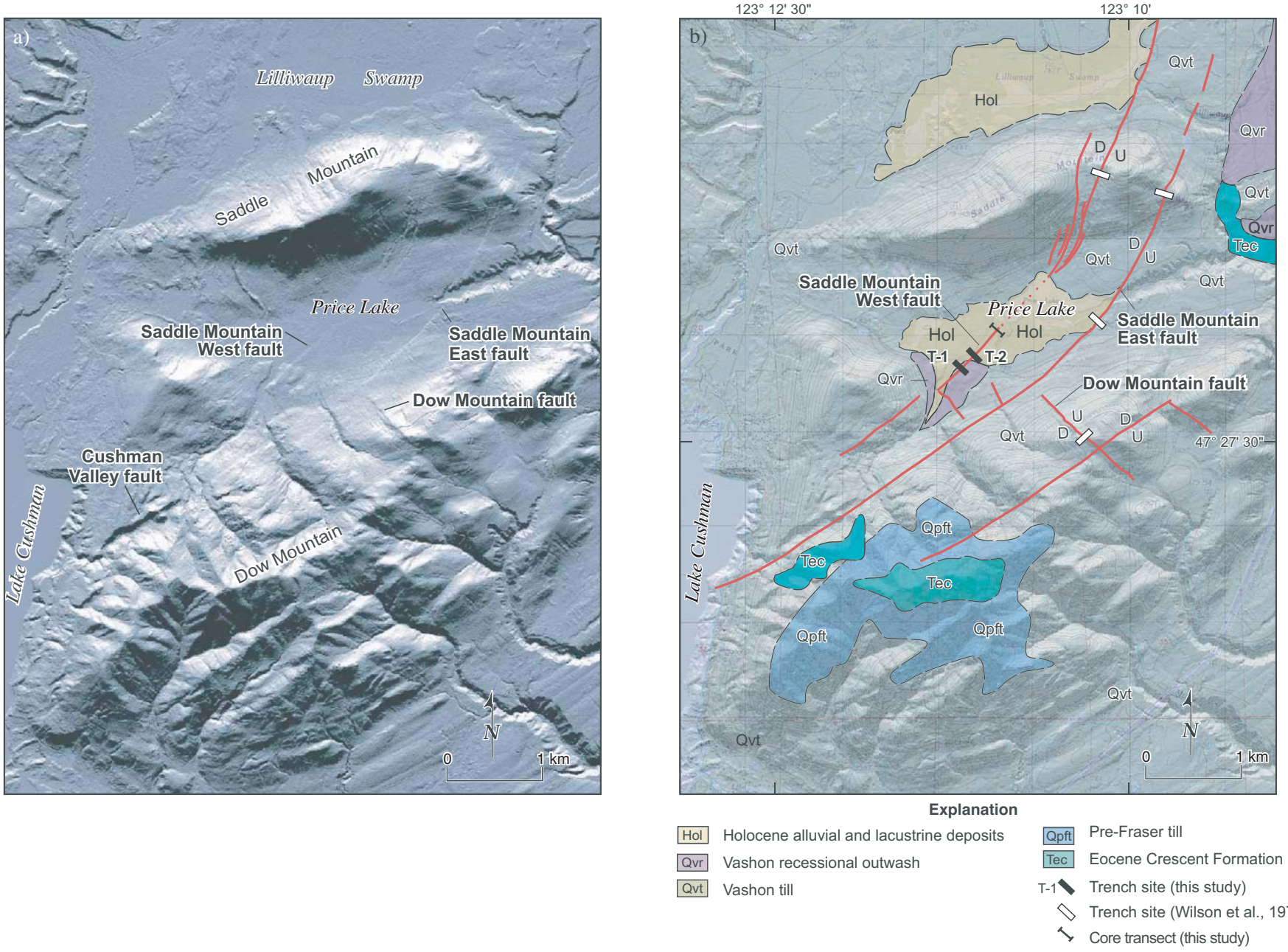

Figure 3. (a) Lidar image of the Price Lake area showing topographic scarps that delineate the Saddle Mountain West, Saddle Mountain East, and Dow Mountain faults previously studied by Wilson et al. (1979). Interpretation of the lidar data has identified additional northeast- and northwest-trending scarps that appear to reflect a coherent system of southeast-dipping reverse faults cut by northwest-striking tear faults. (b) Topographic map of the Price Lake area showing fault scarps interpreted from lidar image at left and Quaternary geology modified from Wilson et al. (1979). The trench sites across the Saddle Mountain West fault are discussed in detail in the text.

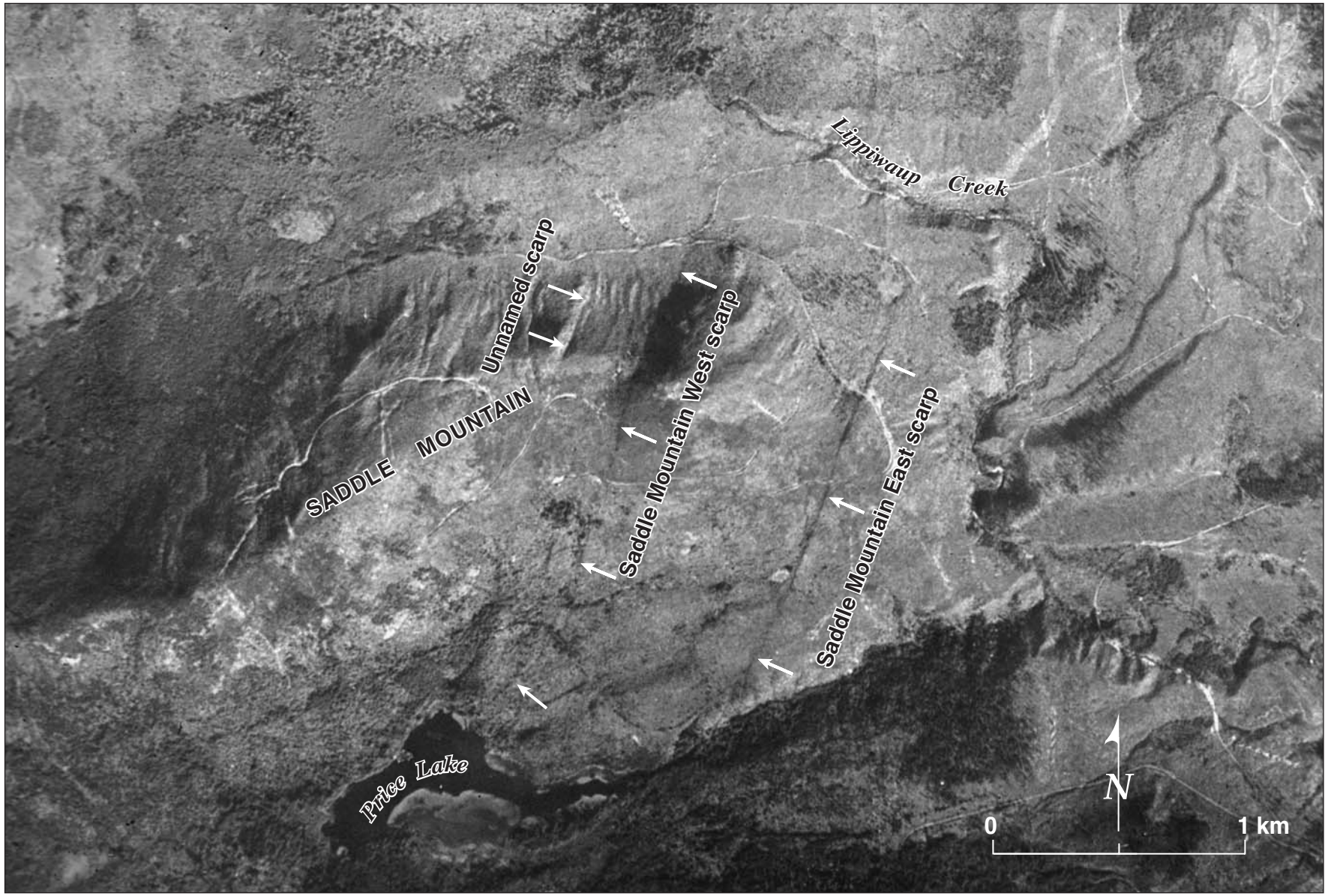

Figure 4. Aerial photograph of Saddle Mountain and Price Lake taken in 1939 shortly after extensive timber harvesting. The denuded landscape reveals several prominent northeast-trending, fault-related scarps including the east-side-up Saddle Mountain West and East scarps, and an unnamed west-side-up scarp that may be an expression of complex deformation related to the western part of the Saddle Mountain fault zone.

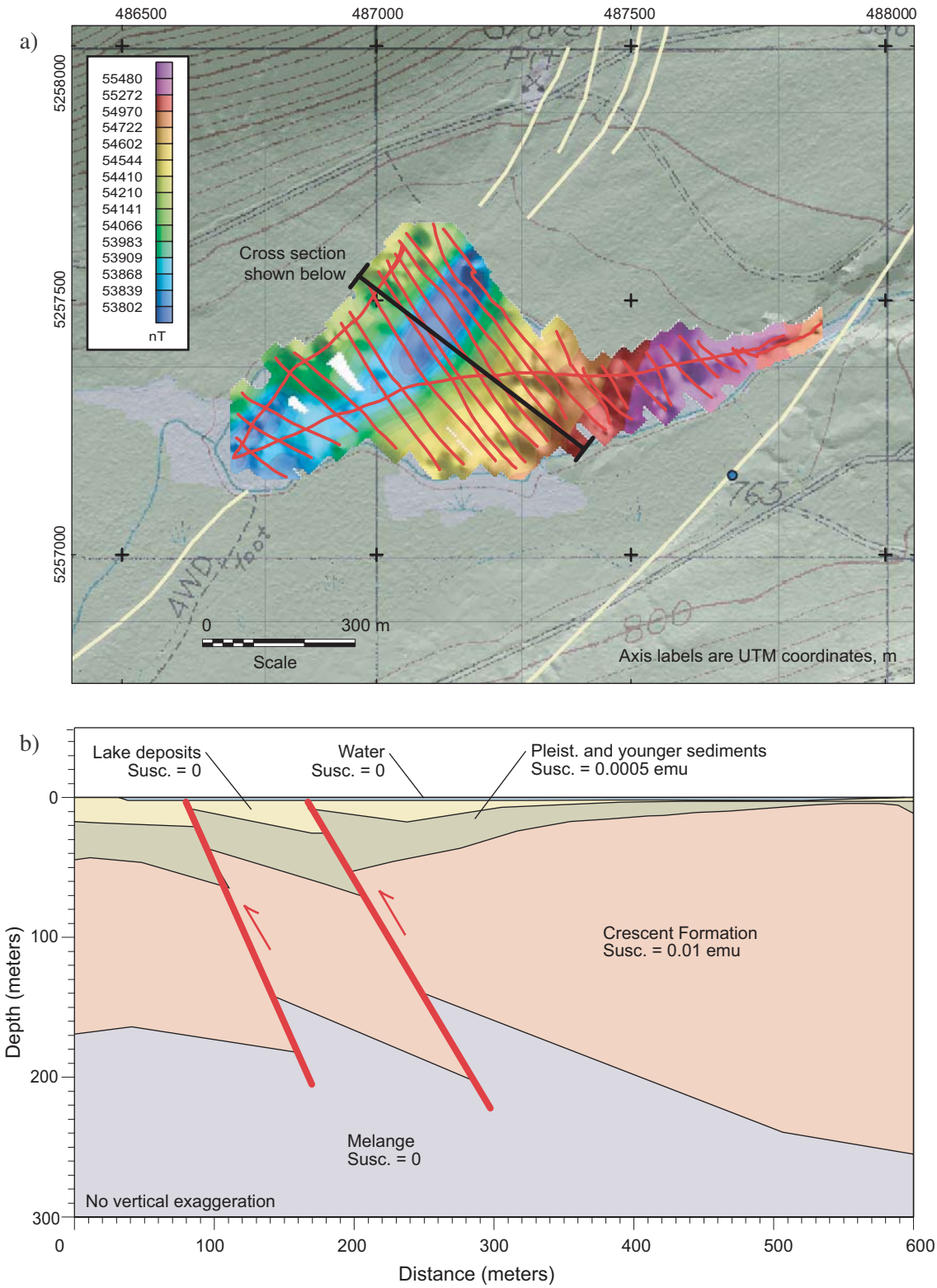

Figure 5. (a) Results of a magnetic survey acquired by canoe on Price Lake (track lines in red) that illuminate a northeast-trending magnetic trough approximately 150 m wide that links topo-graphic scarps (white lines) along the Saddle Mountain West fault. (b) Two-dimensional model consistent with magnetic data that predicts two east-side-up reverse faults in Crescent Formation at >30 m depth (both figures from Blakely et al., 2005).

a)

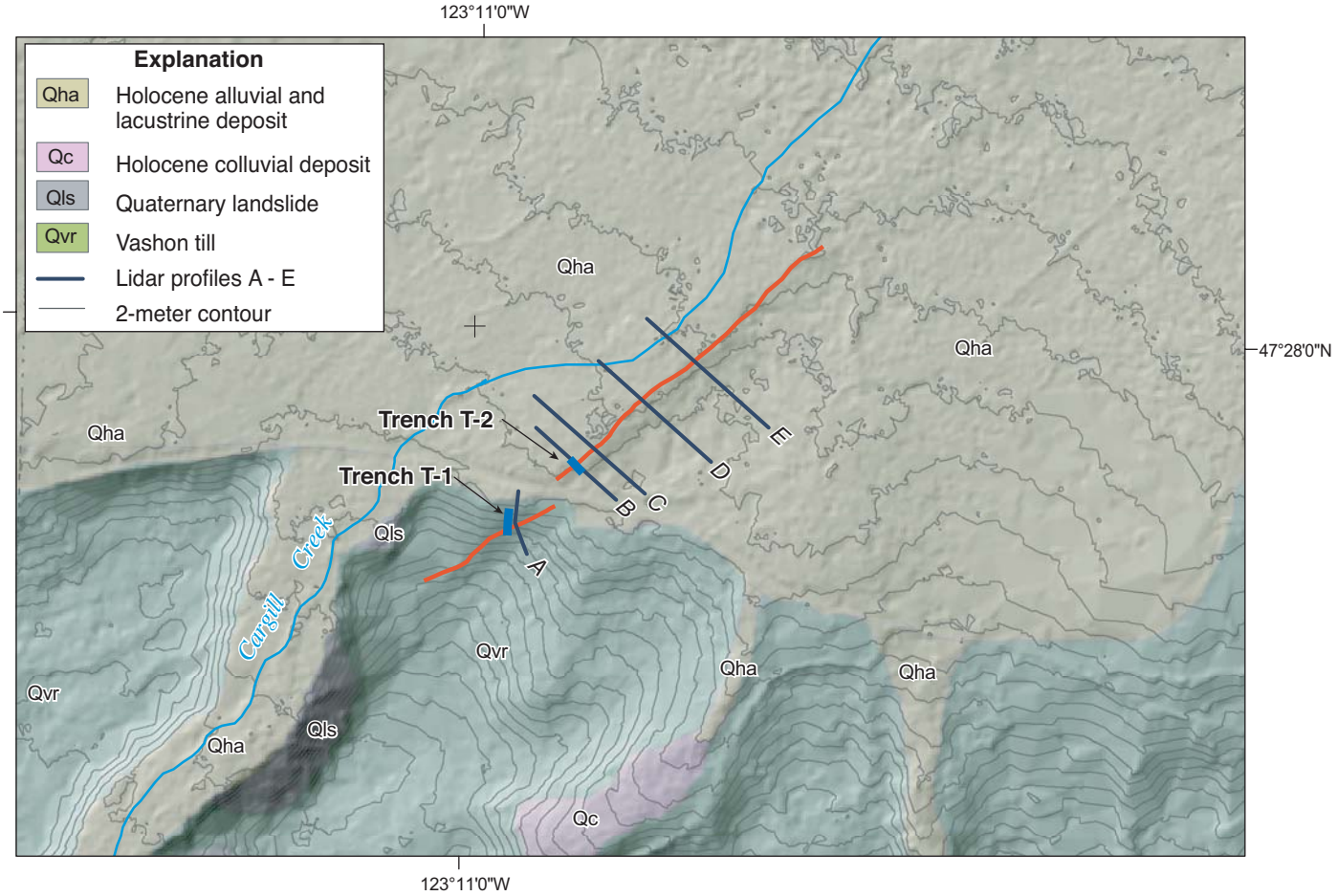

b)

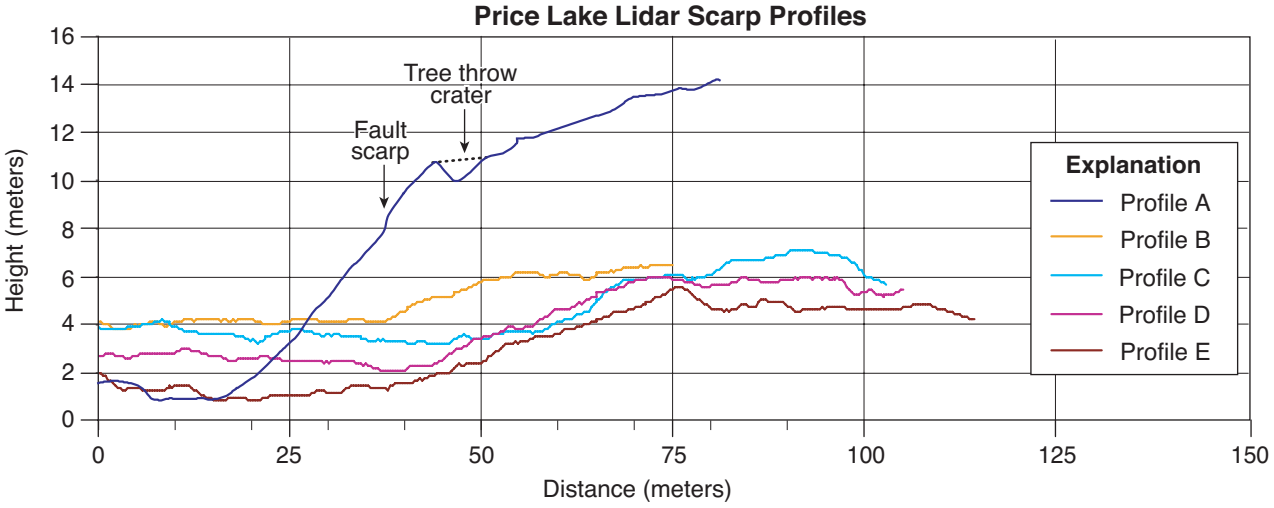

Figure 6. (a) Simplified Quaternary geologic map (modified from Wilson et al., 1979) of the Saddle Mountain West Fault (SMWF) paleoseismic trench sites and ALSM profile locations. Red lines represent the SMWF scarps mapped using tape and compass, total station surveys, and interpretation of ALSM shaded relief images. Note the prominent left step in the trend of the fault scarp possibly caused by erosional modification during logging. Trench 2 was not completed because of safety concerns. The contour interval is 2 meters. (b) Topographic profiles A-E across the SMWF scarps. Profile A developed using both lidar data and trench profile measured in field. Profiles B-E show scarp heights ranging from two meters to greater than four meters. Elevations tied to an arbitrary local datum.

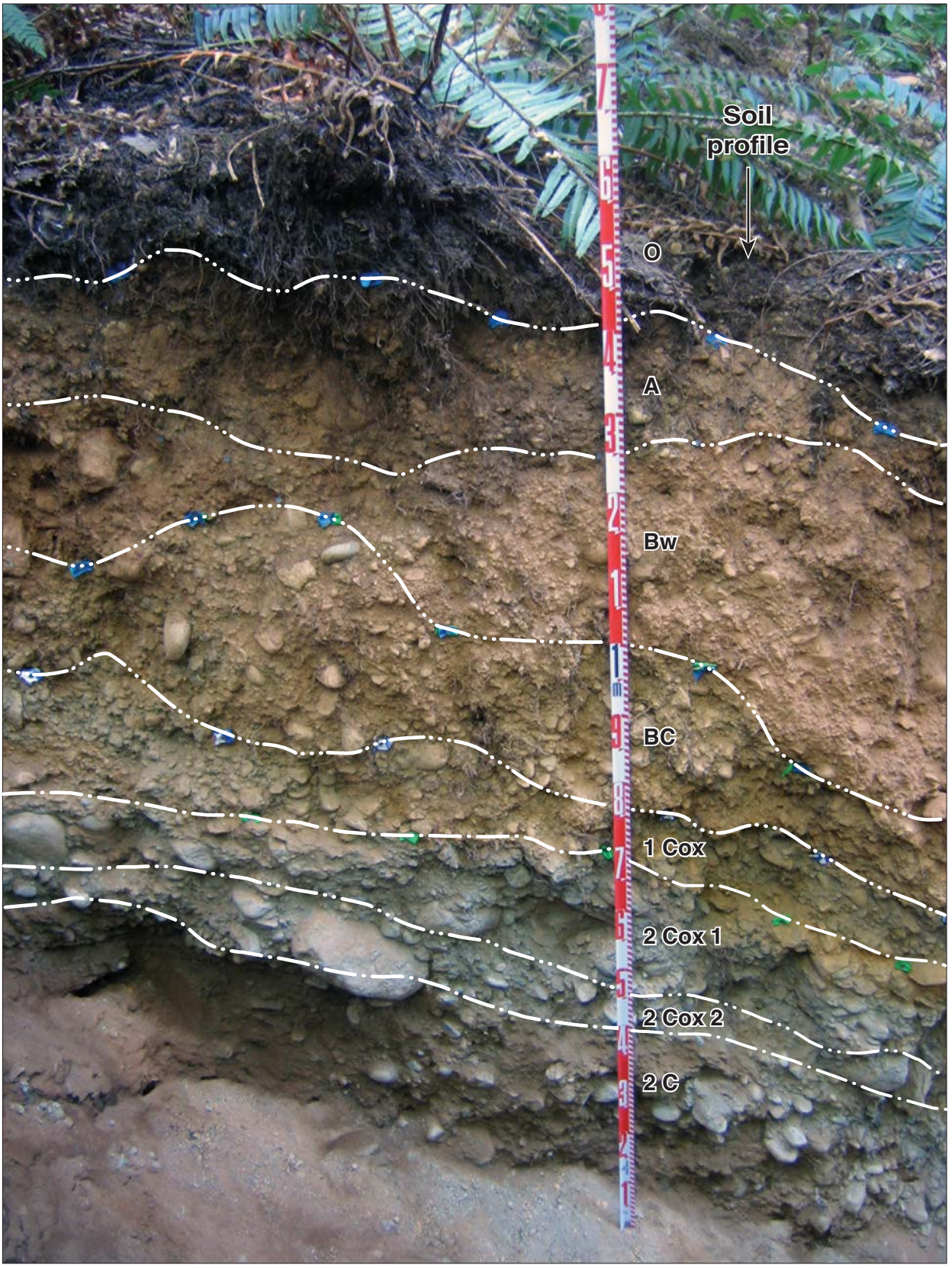

Figure 7. Soil profile, west wall of Cargill Creek trench. Detailed field description of soil profile included in Table 3.

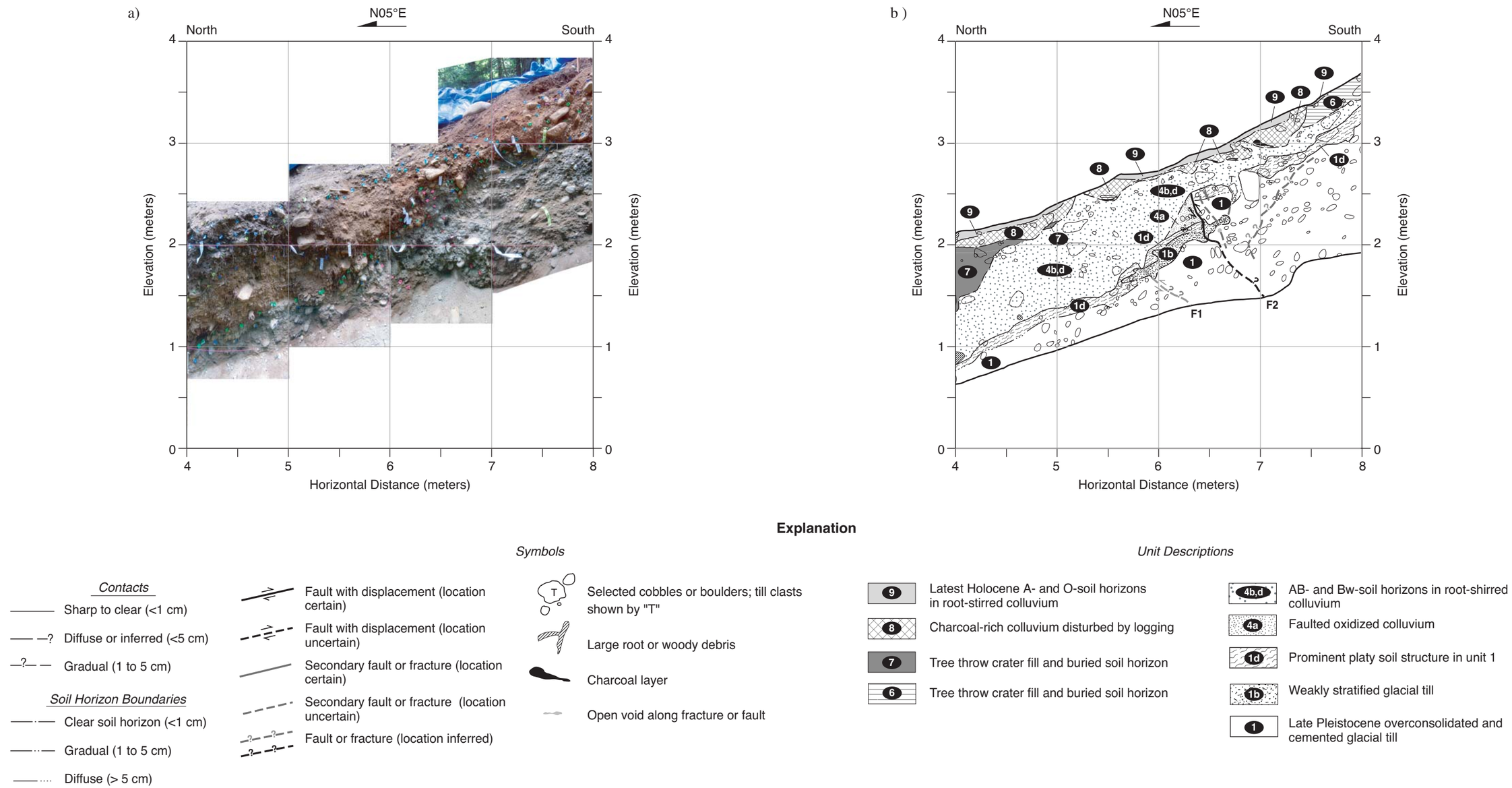

Figure 8. Photomosaic (a) and simplified stratigraphy (b) of the northern third of the Cargill Creek trench eastern wall. Refer to Plate 1 for complete stratigraphic interpretation and Tables 2 and 3 for detailed lithologic and soil descriptions, respectively. Fault F2 offsets Vashon glacial till (unit 1) and overlying oxidized colluvium (unit 4a), but is not coincident with a surface scarp. We infer that slope processes, root stirring and, possibly, early 20th century logging activities obliterated the original scarp.

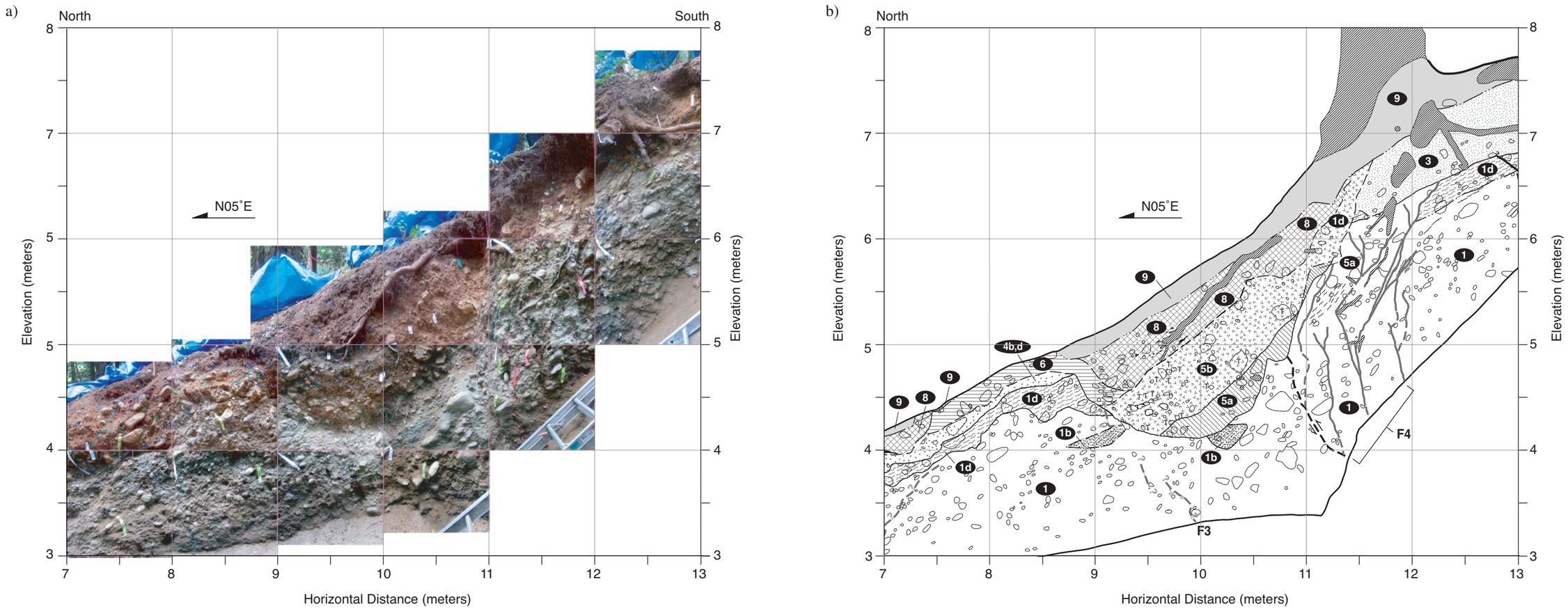

Explanation

Contacts

- Sharp to clear (<1 cm)
- Diffuse or inferred (>5 cm)
- Gradual (1 to 5 cm)

Soil Horizon Boundaries

- Clear soil horizon (<1 cm)
- Gradual (1 to 5 cm)
- Diffuse (> 5 cm)

Symbols

- Fault with displacement (location certain)
- Fault with displacement (location uncertain)
- Secondary fault or fracture (location certain)
- Secondary fault or fracture (location uncertain)
- Fault or fracture (location inferred)
- Selected cobbles or boulders; till clasts shown by "T"
- Large root or woody debris
- Charcoal layer
- Open void along fracture or fault
- Platy soil structure

Unit Descriptions

- 9 — Latest Holocene A- and O-soil horizons in root-stirred colluvium
- 8 — Charcoal-rich colluvium disturbed by logging
- 6 — Tree throw crater fill and scarp colluvium
- 5b — Scarp colluvium derived from erosion of units 1 and 3
- 5a — Scarp colluvium derived from collapse of unit 1
- 4b,d — AB- and Bw-soil horizons in root-shirred colluvium
- 3 — Bw- and C-soil horizons in root-stirred colluvium
- 1d — Prominent platy soil structure in unit 1
- 1b — Weakly stratified glacial till
- 1 — Late Pleistocene overconsolidated and cemented glacial til

Figure 9. Photomosaic (a) and simplified stratigraphy (b) of the central third of the Cargill Creek trench eastern wall. Refer to Plate 1 for complete stratigraphic interpretation and Tables 2 and 3 for detailed lithologic and soil descriptions, respectively. Fault F3 is inferred from aligned fractures and open voids in glacial till. Friable, probably sheared glacial till, fractures in till and open voids characterize fault zone F4. Together, fault F3 and fault zone F4 define the margins of an inferred down-dropped block located below scarp derived colluvium (unit 5).

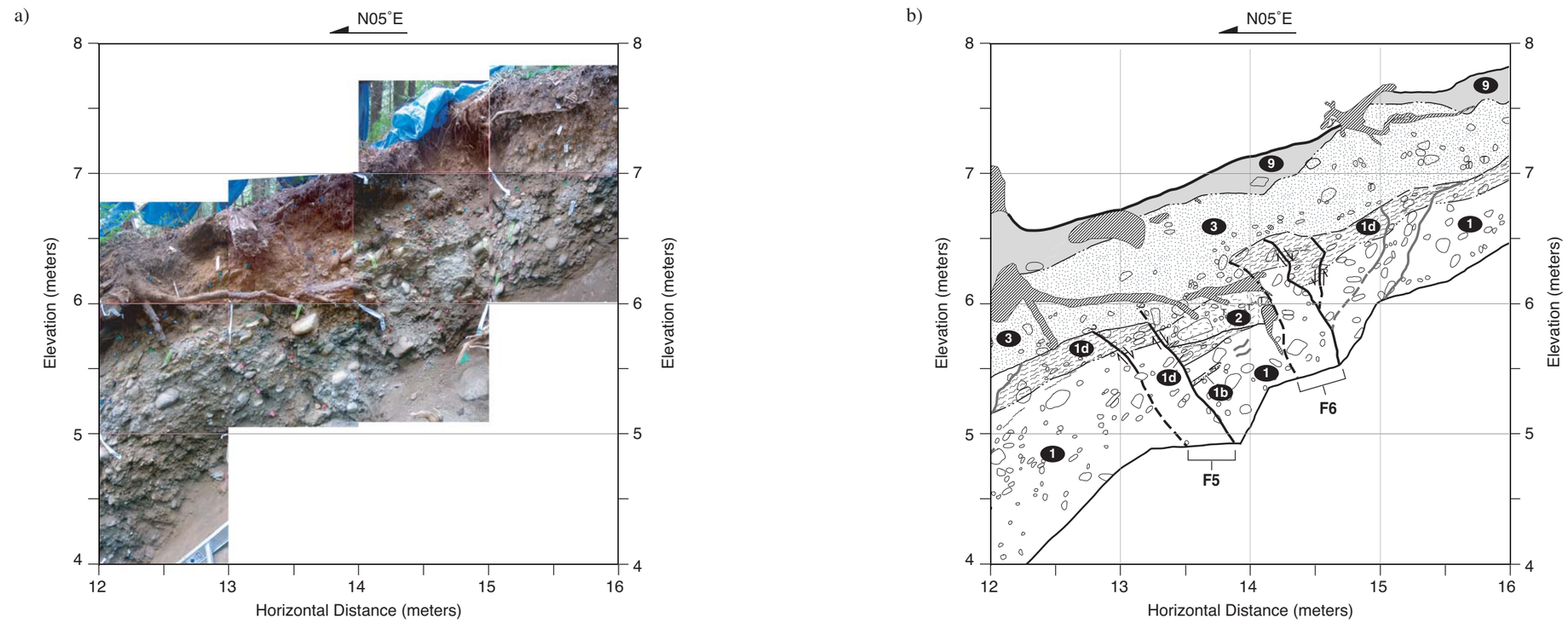

Explanation

Contacts

- Sharp to clear (<1 cm)
- Diffuse or inferred (>5 cm)
- Gradual (1 to 5 cm)

Soil Horizon Boundaries

- Clear soil horizon (<1 cm)
- Gradual (1 to 5 cm)
- Diffuse (> 5 cm)

Symbols

- Fault with displacement (location certain)
- Fault with displacement (location uncertain)
- Secondary fault or fracture (location certain)
- Secondary fault or fracture (location uncertain)
- Fault or fracture (location inferred)
- Selected cobbles or boulders; till clasts shown by "T"
- Large root or woody debris
- Charcoal layer
- Open void along fracture or fault
- Platy soil structure

Unit Descriptions

- 9 — Latest Holocene A- and O-soil horizons in root-stirred colluvium
- 3 — Bw- and C-soil horizons in root-stirred colluvium
- 2 — Stratified gravelly silt and sand
- 1d — Prominent platy soil structure in unit 1
- 1b — Weakly stratified glacial till
- 1 — Late Pleistocene overconsolidated and cemented glacial till

Figure 10. Photomosaic (a) and simplified stratigraphy (b) of the southern third of the Cargill Creek trench eastern wall. Refer to Plate 1 for complete stratigraphic interpretation and Tables 2 and 3 for detailed lithologic and soil descriptions, respectively. Faults F5 and F6 offset glacial till, stratified deposits of unit 2 and the lowest soil horizon of unit 3. These faults are coincident with a beveled surface above the main scarp and define a down-dropped block that prevented bedding in unit 2 from being homogenized by slope processes and root-stirring. Therefore, we infer that slip on faults F5 and F6 occurred prior to movement on faults exposed in the trench to the north that formed the main scarp.

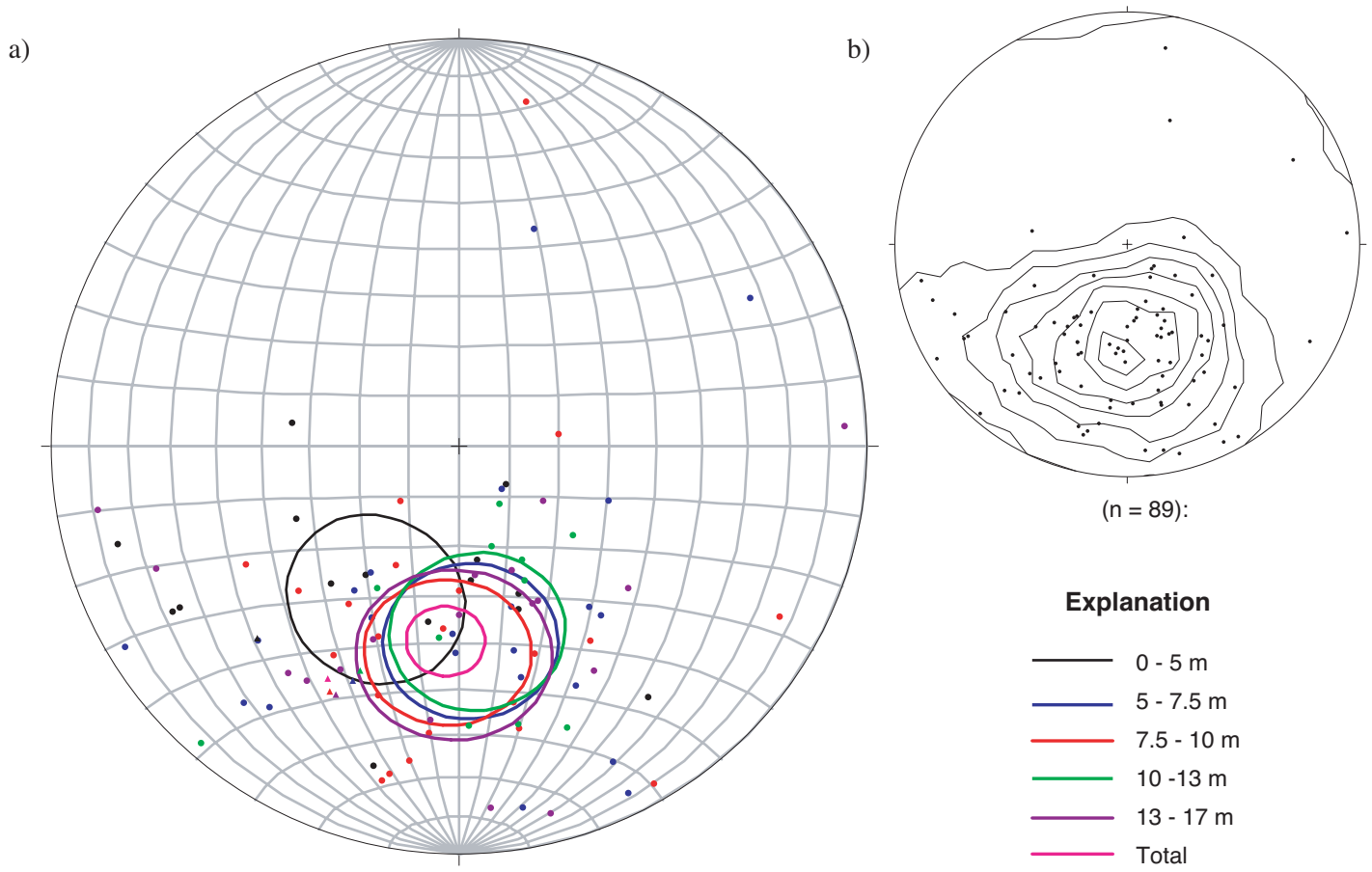

Figure 11. Lower hemisphere equal area stereonet projections of 89 clast orientation measurements in the Vashon Till. (a) Poles to clast orientations are divided into 5 groups assigned different colors that correspond to cobble measurements from six separate but adjacent sections of the trench wall defined by horizontal distance in the key. Mean pole calculations and 95% confidence intervals shown by small circles with the same colors (see table 5) . (b) Kamb contours of all clast measurements reveal a consistent pole concentration in the southern quadrant. This plot suggests a generally east-striking and north-dipping cobble fabric in the till. Kamb contour intervals for the density of cobble orientation poles are in multiples of standard deviations above a random data set. The base contours interval is 3 standard deviations.

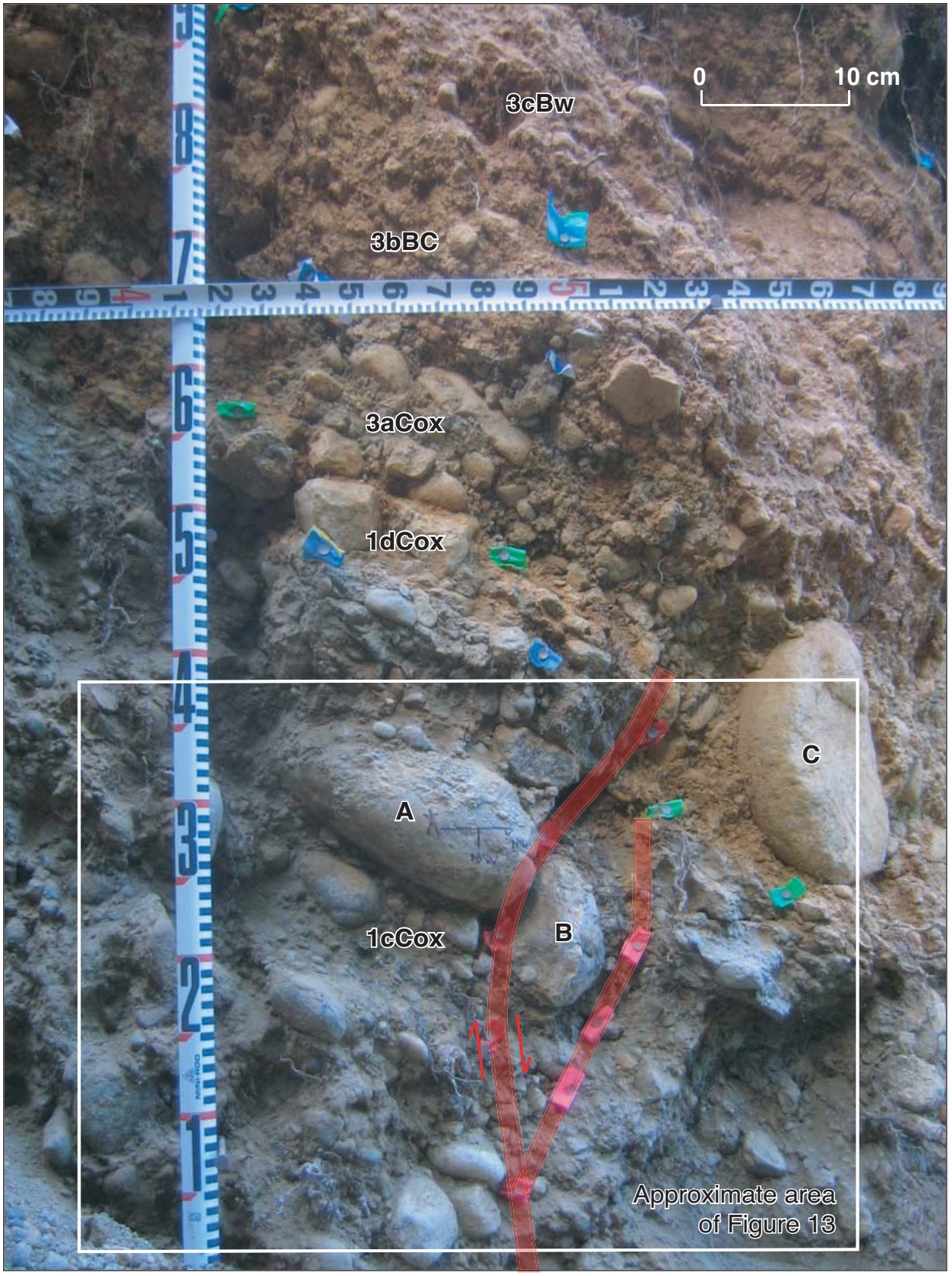

Figure 12. Photograph showing an offset basalt cobble exposed on the west wall of the Cargill Creek trench with slip indicators consistent with right-lateral oblique reverse displacement on fault F6.1. Cobbles "A" and "B" are two pieces of a formerly (presumed) intact 28-cm long cobble. The cobble is offset by fault F6.1. Both cobble fragments were firmly cemented in unit 1 and showed no evidence for rotation. In contrast, a 22.5-cm long cobble ("C") in overlying unit 3c appears to be significantly rotated from its original position. The strike of the axial plane of cobble "C" is N 47° W with a dip of 88° NE. Geologic unit labels indicate correlative units on east trench wall. Approximate location of photo center is opposite station 14.5 m, 5.5 m on the east wall. Vertical ruler in tenths of meters; horizontal ruler in tenths of feet.

Figure 13. Close up photograph of offset cobble showing piercing line used to estimate slip vector. The fault strikes N 47° E and dips 58° S. Displacement of the piercing point is 7.5 cm with a rake of 51° to 56° NE in the plane of the fault.

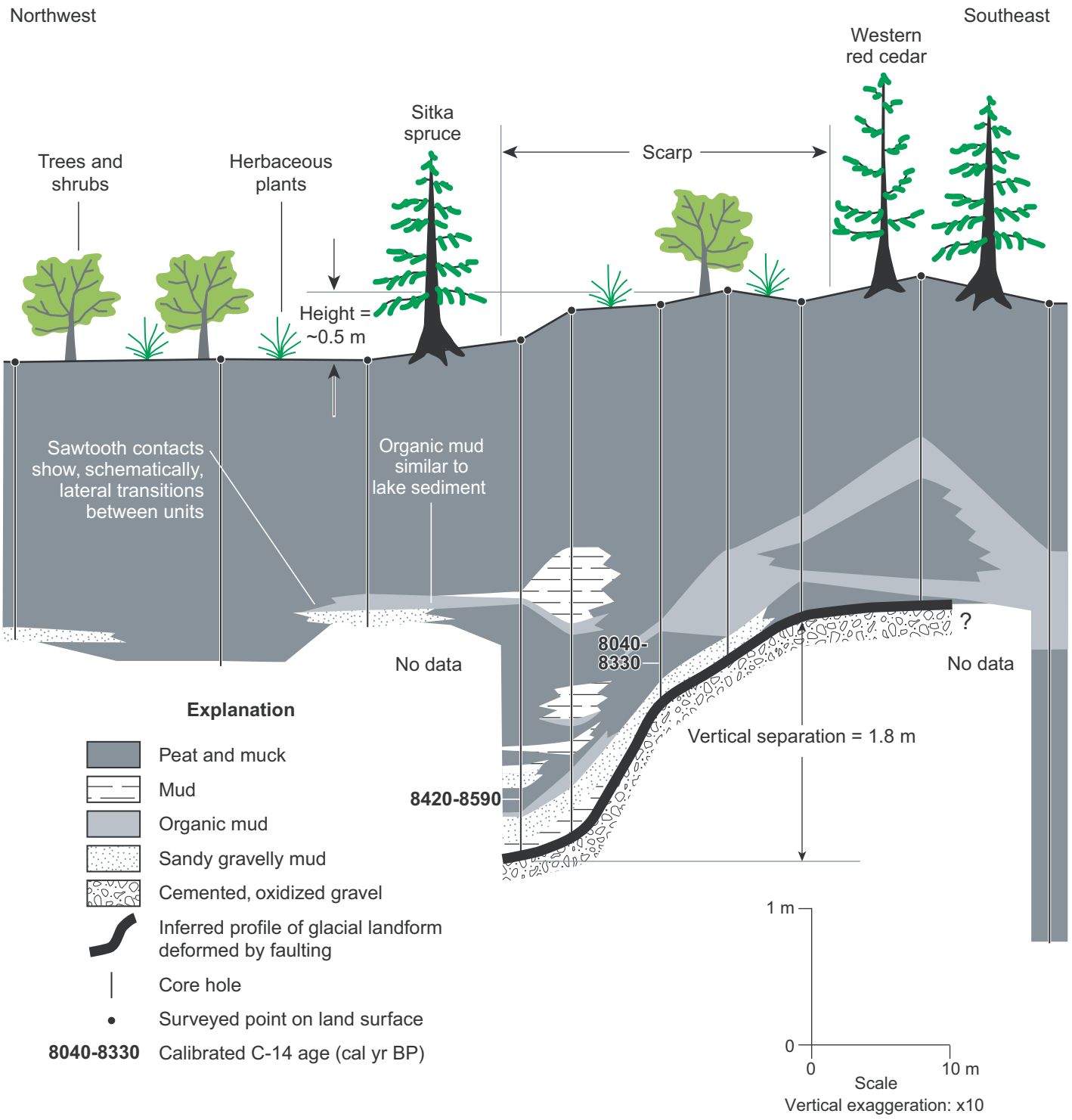

Figure 14. Stratigraphic profile depicting a 76-m-long sediment core transect across the projected trace of the Saddle Mountain West fault, located approximately 100-m southwest of Price Lake (see Figure 3). Core site elevation and location surveyed to an arbitrary datum with hand level and tape. Post-glacial movement of the West fault is inferred from the surface scarp and northwestward-thickening sediments, both which are consistent with south-side-up deformation across the scarp. The top of cemented, oxidized gravel (bold line), interpreted as glacial outwash, shows a vertical separation of about 1.8 m across the projected fault trace. At the surface, the scarp is approximately 0.5 m high. Complex stratigraphic relations and core refusal on coarse material at most core sites permit an alternative explanation for the apparent vertical offset of the top of outwash involving post-glacial fluvial scouring.

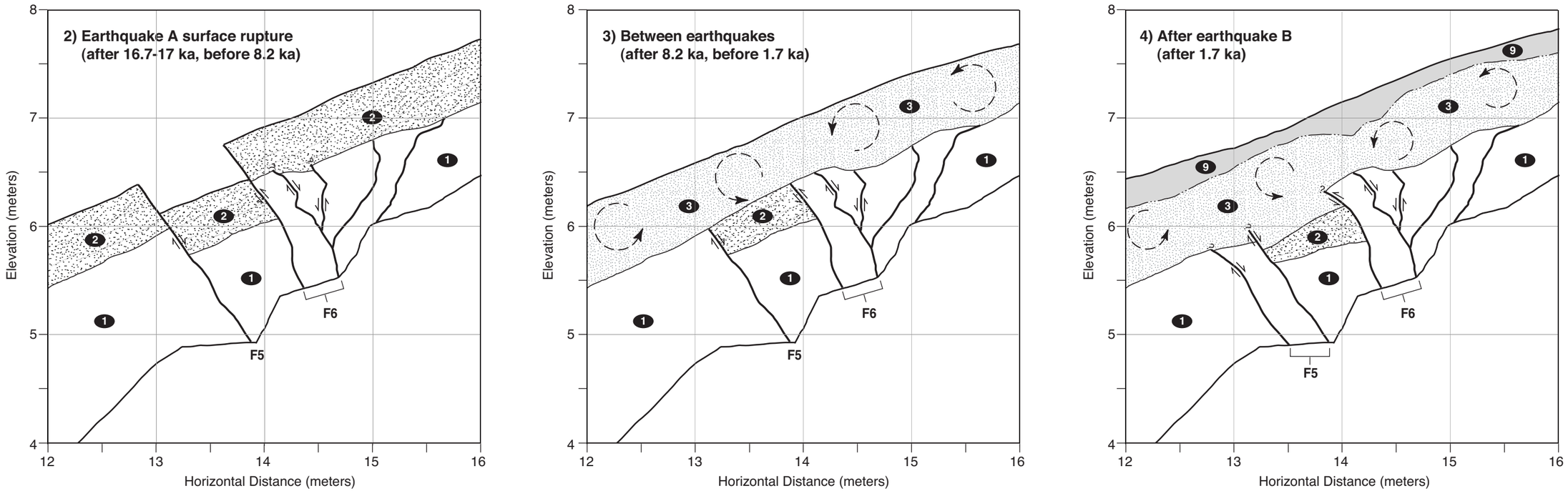

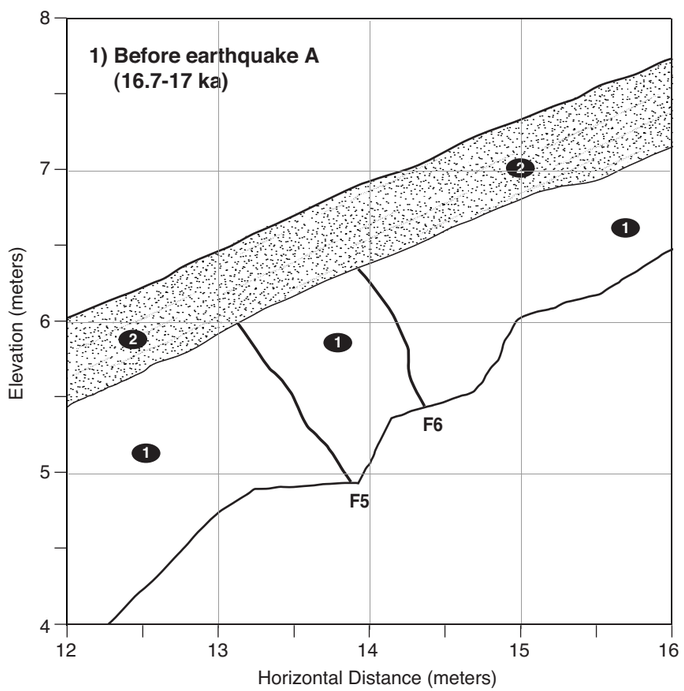

Explanation

Symbols

- Fault or fracture
- Stratigraphic contact
- Soil horizon boundary
- Mixing by slope and soil processes

Unit Descriptions

- 9 — Latest Holocene A- and O-soil horizons
- 3 — Colluvium stirred by slope and soil processes
- 2 — Stratified glacial drift or recessional outwash
- 1 — Vashon glacial till

Figure 15. Schematic reconstruction of earthquake surface ruptures at Cargill Creek inferred from retrodeforming stratigraphic units along faults in the southern part of the trench. Unit numbers from trench log (Plate 1) with simplified descriptions. Median age constraints from calibrated radiocarbon data listed in Table 5 and discussed in text. Panel 1 depicts a conceptual post-glacial landscape formed by stratified drift (unit 2) over glacial till (unit 1) prior to earthquake A. Panel 2 shows the instantaneous surface rupture inferred for earthquake A that created a small graben bound by faults F5 and F6 . Other faults directly south of the down-dropped block also may have offset the lower contact of unit 2. In panel 3, slope and soil processes active between earthquakes destroy the original stratification of unit 2 and produce colluvial deposits and soil horizons of unit 3. Relict stratification in the faulted remnant of unit 2 is preserved because the fault block dropped below the nominal depth of colluvial mixing. Reactivation of faults F5 and F6 during earthquake B, shown in panel 4, offsets the base of unit 3. Slope and soil processes active after earthquake B continue to mix unit 3 and destroy stratigraphic evidence of surface rupture.

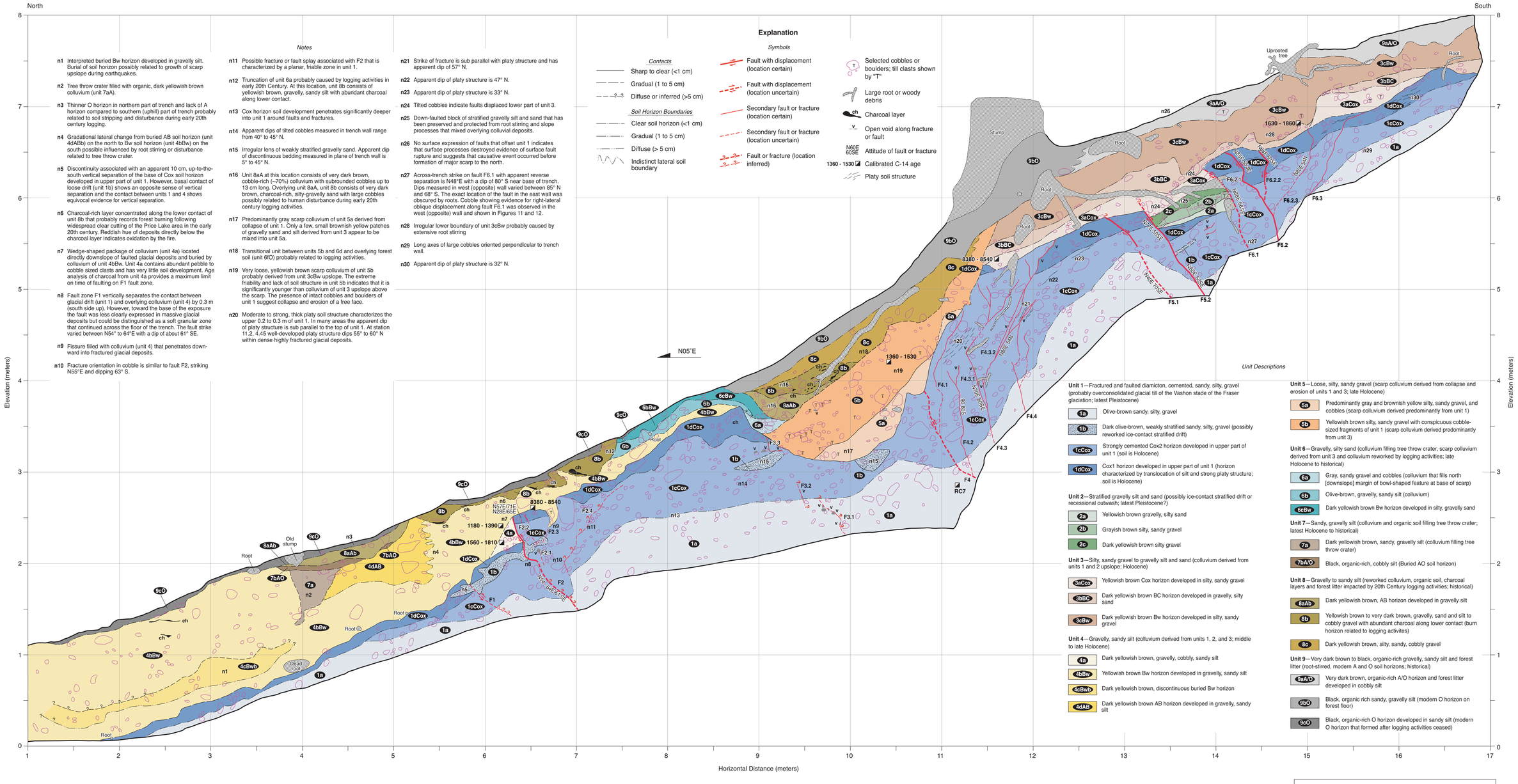

Notes

n1 Interpreted buried Bw horizon developed in gravelly silt. Burial of soil horizon possibly related to growth of scarp upslope during earthquakes.

n2 Tree throw crater filled with organic, dark yellowish brown colluvium (unit 7aA).

n3 Thinner O horizon in northern part of trench and lack of A horizon compared to southern (uphill) part of trench probably related to soil stripping and disturbance during early 20th century logging.

n4 Gradational lateral change from buried AB soil horizon (unit 4dABb) on the north to Bw soil horizon (unit 4bBw) on the south possible influenced by root stirring or disturbance related to tree throw crater.

n5 Discontinuity associated with an apparent 10 cm, up-to-the-south vertical separation of the base of Cox soil horizon developed in upper part of unit 1. However, basal contact of loose drift (unit 1b) shows an opposite sense of vertical separation and the contact between units 1 and 4 shows equivocal evidence for vertical separation.

n6 Charcoal-rich layer concentrated along the lower contact of unit 8b that probably records forest burning following widespread clear cutting of the Price Lake area in the early 20th century. Reddish hue of deposits directly below the charcoal layer indicates oxidation by the fire.

n7 Wedge-shaped package of colluvium (unit 4a) located directly downslope of faulted glacial deposits and buried by colluvium of unit 4bBw. Unit 4a contains abundant pebble to cobble sized clasts and has very little soil development. Age analysis of charcoal from unit 4a provides a maximum limit on time of faulting on F1 fault zone.

n8 Fault zone F1 vertically separates the contact between glacial drift (unit 1) and overlying colluvium (unit 4) by 0.3 m (south side up). However, toward the base of the exposure the fault was less clearly expressed in massive glacial deposits but could be distinguished as a soft granular zone that continued across the floor of the trench. The fault strike varied between N54° to 64°E with a dip of about 61° SE.

n9 Fissure filled with colluvium (unit 4) that penetrates downward into fractured glacial deposits.

n10 Fracture orientation in cobble is similar to fault F2, striking N55°E and dipping 63° S.

n11 Possible fracture or fault splay associated with F2 that is characterized by a planar, friable zone in unit 1.

n12 Truncation of unit 6a probably caused by logging activities in early 20th Century. At this location, unit 8b consists of yellowish brown, gravelly, sandy silt with abundant charcoal along lower contact.

n13 Cox horizon soil development penetrates significantly deeper into unit 1 around faults and fractures.

n14 Apparent dips of tilted cobbles measured in trench wall range from 40° to 45° N.

n15 Irregular lens of weakly stratified gravelly sand. Apparent dip of discontinuous bedding measured in plane of trench wall is 5° to 45° N.

n16 Unit 8aA at this location consists of very dark brown, cobble-rich (~70%) colluvium with subrounded cobbles up to 13 cm long. Overlying unit 8aA, unit 8b consists of very dark brown, charcoal-rich, silty-gravelly sand with large cobbles possibly related to human disturbance during early 20th century logging activities.

n17 Predominantly gray scarp colluvium of unit 5a derived from collapse of unit 1. Only a few, small brownish yellow patches of gravelly sand and silt derived from unit 3 appear to be mixed into unit 5a.

n18 Transitional unit between units 5b and 6d and overlying forest soil (unit 6fO) probably related to logging activities.

n19 Very loose, yellowish brown scarp colluvium of unit 5b probably derived from unit 3cBw upslope. The extreme friability and lack of soil structure in unit 5b indicates that it is significantly younger than colluvium of unit 3 upslope above the scarp. The presence of intact cobbles and boulders of unit 1 suggest collapse and erosion of a free face.

n20 Moderate to strong, thick platy soil structure characterizes the upper 0.2 to 0.3 m of unit 1. In many areas the apparent dip of platy structure is sub parallel to the top of unit 1. At station 11.2, 4.45 well-developed platy structure dips 55° to 60° N within dense highly fractured glacial deposits.

n21 Strike of fracture is sub parallel with platy structure and has apparent dip of 57° N.

n22 Apparent dip of platy structure is 47° N.

n23 Apparent dip of platy structure is 33° N.

n24 Tilted cobbles indicate faults displaced lower part of unit 3.

n25 Down-faulted block of stratified gravelly silt and sand that has been preserved and protected from root stirring and slope processes that mixed overlying colluvial deposits.

n26 No surface expression of faults that offset unit 1 indicates that surface processes destroyed evidence of surface fault rupture and suggests that causative event occurred before formation of major scarp to the north.

n27 Across-trench strike on fault F6.1 with apparent reverse separation is N48°E with a dip of 80° S near base of trench. Dips measured in west (opposite) wall varied between 85° N and 68° S. The exact location of the fault in the east wall was obscured by roots. Cobble showing evidence for right-lateral oblique displacement along fault F6.1 was observed in the west (opposite) wall and shown in Figures 11 and 12.

n28 Irregular lower boundary of unit 3cBw probably caused by extensive root stirring

n29 Long axes of large cobbles oriented perpendicular to trench wall.

n30 Apparent dip of platy structure is 32° N.

Explanation

Contacts

- Sharp to clear (<1 cm)
- Gradual (1 to 5 cm)
- Diffuse or inferred (>5 cm)

Soil Horizon Boundaries

- Clear soil horizon (<1 cm)
- Gradual (1 to 5 cm)
- Diffuse (> 5 cm)
- Indistinct lateral soil boundary

Symbols

- Fault with displacement (location certain)
- Fault with displacement (location uncertain)
- Secondary fault or fracture (location certain)
- Secondary fault or fracture (location uncertain)
- Fault or fracture (location inferred)
- Selected cobbles or boulders; till clasts shown by "T"
- Large root or woody debris
- ch — Charcoal layer
- v — Open void along fracture or fault
- N60E 60SE — Attitude of fault or fracture
- 1360 - 1530 — Calibrated C-14 age
- Platy soil structure

Unit Descriptions

Unit 1—Fractured and faulted diamicton, cemented, sandy, silty, gravel (probably overconsolidated glacial till of the Vashon stade of the Fraser glaciation; latest Pleistocene)

- **1a** Olive-brown sandy, silty, gravel
- **1b** Dark olive-brown, weakly stratified sandy, silty, gravel (possibly reworked ice-contact stratified drift)
- **1cCox** Strongly cemented Cox2 horizon developed in upper part of unit 1 (soil is Holocene)
- **1dCox** Cox1 horizon developed in upper part of unit 1 (horizon characterized by translocation of silt and strong platy structure; soil is Holocene)

Unit 2—Stratified gravelly silt and sand (possibly ice-contact stratified drift or recessional outwash; latest Pleistocene?)

- **2a** Yellowish brown gravelly, silty sand
- **2b** Grayish brown silty, sandy gravel
- **2c** Dark yellowish brown silty gravel

Unit 3—Silty, sandy gravel to gravelly silt and sand (colluvium derived from units 1 and 2 upslope; Holocene)

- **3aCox** Yellowish brown Cox horizon developed in silty, sandy gravel
- **3bBC** Dark yellowish brown BC horizon developed in gravelly, silty sand
- **3cBw** Dark yellowish brown Bw horizon developed in silty, sandy gravel

Unit 4—Gravelly, sandy silt (colluvium derived from units 1, 2, and 3; middle to late Holocene)

- **4a** Dark yellowish brown, gravelly, cobbly, sandy silt
- **4bBw** Yellowish brown Bw horizon developed in gravelly, sandy silt
- **4cBwb** Dark yellowish brown, discontinuous buried Bw horizon
- **4dAB** Dark yellowish brown AB horizon developed in gravelly, sandy silt

Unit 5—Loose, silty, sandy gravel (scarp colluvium derived from collapse and erosion of units 1 and 3; late Holocene)

- **5a** Predominantly gray and brownish yellow silty, sandy gravel, and cobbles (scarp colluvium derived predominantly from unit 1)
- **5b** Yellowish brown silty, sandy gravel with conspicuous cobble-sized fragments of unit 1 (scarp colluvium derived predominantly from unit 3)

Unit 6—Gravelly, silty sand (colluvium filling tree throw crater, scarp colluvium derived from unit 3 and colluvium reworked by logging activities; late Holocene to historical)

- **6a** Gray, sandy gravel and cobbles (colluvium that fills north [downslope] margin of bowl-shaped feature at base of scarp)
- **6b** Olive-brown, gravelly, sandy silt (colluvium)
- **6cBw** Dark yellowish brown Bw horizon developed in silty, gravelly sand

Unit 7—Sandy, gravelly silt (colluvium and organic soil filling tree throw crater; latest Holocene to historical)

- **7a** Dark yellowish brown, sandy, gravelly silt (colluvium filling tree throw crater)
- **7bA/O** Black, organic-rich, cobbly silt (Buried AO soil horizon)

Unit 8—Gravelly to sandy silt (reworked colluvium, organic soil, charcoal layers and forest litter impacted by 20th Century logging activities; historical)

- **8aAb** Dark yellowish brown, AB horizon developed in gravelly silt
- **8b** Yellowish brown to very dark brown, gravelly, sand and silt to cobbly gravel with abundant charcoal along lower contact (burn horizon related to logging activites)
- **8c** Dark yellowish brown, silty, sandy, cobbly gravel

Unit 9—Very dark brown to black, organic-rich gravelly, sandy silt and forest litter (root-stirred, modern A and O soil horizons; historical)

- **9aA/O** Very dark brown, organic-rich A/O horizon and forest litter developed in cobbly silt
- **9bO** Black, organic rich sandy, gravelly silt (modern O horizon on forest floor)
- **9cO** Black, organic-rich O horizon developed in sandy silt (modern O horizon that formed after logging activities ceased)

S A D D L E M O U N T A I N

Trench T-1
East Wall

WLA William Lettis & Associates, Inc.

Plate 1

1720 Price Lake

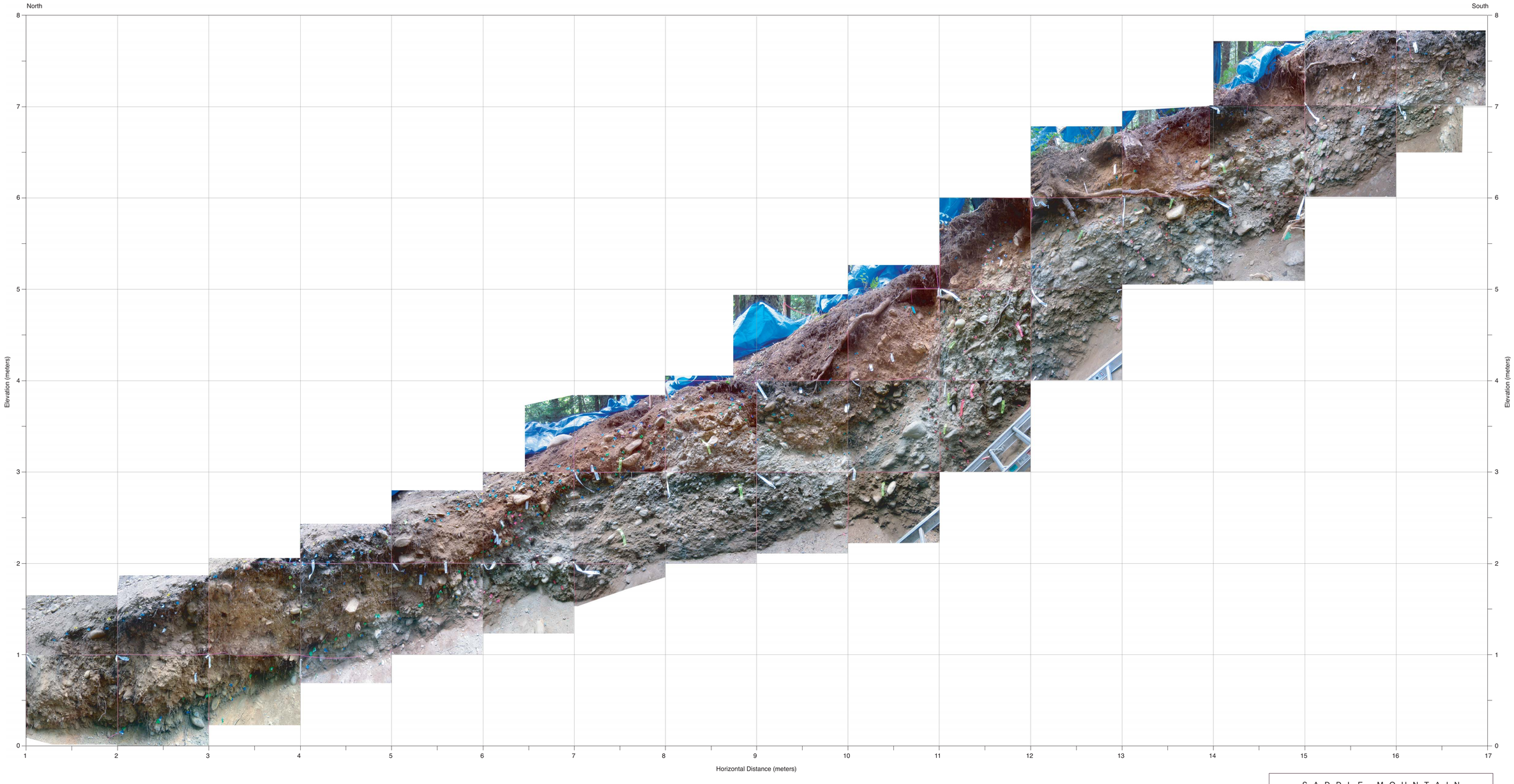

S A D D L E M O U N T A I N

Photomosaic of Trench T-1

WLA William Lettis & Associates, Inc. | Plate 2

1720 Price Lake